A Multiplicative Calderon Preconditioner for the Electric Field Integral Equation

Francesco P. Andriulli, Kristof Cools, Hakan Bağci, Femke Olyslager, *Fellow, IEEE*, Annalisa Buffa, Snorre Christiansen, and Eric Michielssen, *Fellow, IEEE*

***Abstract*—In this paper, a new technique for preconditioning electric field integral equations (EFIEs) by leveraging Calderón identities is presented. In contrast to all previous Calderón preconditioners, the proposed preconditioner is purely multiplicative in nature, applicable to open and closed structures, straightforward to implement, and easily interfaced with existing method of moments (MoM) code. Numerical results demonstrate that the MoM EFIE system obtained using the proposed preconditioning converges rapidly, independently of the discretization density.**

***Index Terms*—Electric field integral equation (EFIE), integral equations, numerical methods, preconditioning.**

I. Introduction

METHOD OF MOMENTS (MoM)-based electric field integral equation (EFIE) solvers are widely used for analyzing time-harmonic electromagnetic radiation and scattering from perfect electrically conducting (PEC) surfaces [1]. These solvers' popularity stems from the fact that they only require surface discretizations, operate on (comparatively) small interaction matrices that can be applied rapidly to arbitrary vectors by using fast multipole and related algorithms [2]–[4], and yield solutions that automatically satisfy the radiation condition. That said, EFIE MoM solvers are no panacea. Indeed, the singular values of the EFIE operator comprise two branches, one accumulating at zero and the other at infinity [5]. The condition numbers of EFIE MoM interaction matrices, therefore, grow rapidly with the surface discretization density. As a result, these matrices often are ill-conditioned, thereby compromising the EFIE MoM solvers' accuracy when applied to structures with subwavelength geometric features.

Manuscript received September 7, 2007; revised December 13, 2007. Published August 6, 2008 (projected). This work was supported by the Air Force Office of Scientific Research under Grant MURI F014432-051936, by the National Science Foundations under Grant DMS 0713771, by the Defense Advanced Research Projects Agency under Grant DSO/AFOSR F015123-052587, and by the Semiconductor Research Corporation under Grant 2006-01385-01.

F. P. Andriulli was with the Electrical Engineering and Computer Science Department, University of Michigan, Ann Arbor, MI USA. He is now with the Politecnico di Torino, Torino 10100, Italy (e-mail: fandri@umich.edu)

H. Bağci and E. Michielssen are with the Electrical Engineering and Computer Science Department, University of Michigan, Ann Arbor, MI 48109 USA.

K. Cools and F. Olyslager are with the Department of Information Technology (INTEC), Ghent University, B-9000 Ghent, Belgium.

A. Buffa is with the Instituto di Matematica Applicata e Tecnologie Informatiche, Italian National Research Council (CNR), Pavia 27100, Italy.

S. Christiansen is with the Centre of Mathematics for Applications, Department of Mathematics, University of Oslo, Oslo, Norway.

Color versions of one or more of the figures in this paper are available online at http://ieeexplore.ieee.org.

Digital Object Identifier 10.1109/TAP.2008.926788

The recent literature abounds with techniques for preconditioning EFIEs by leveraging Calderón identities [6]–[9]. These techniques exploit the self-regularizing property of the EFIE, i.e., the fact that the square of the EFIE operator does not have eigenvalues accumulating at zero or infinity. Calderón-preconditioned EFIEs give rise to MoM matrices that are well conditioned, independent of the discretization density. Unfortunately, none of the Calderón preconditioners proposed to date are easily integrated into existing MoM codes. Invariably, implementation bottlenecks can be traced to the need to construct a well-conditioned Gram matrix linking the domain and range of the EFIE operator, as is required when discretizing EFIE·EFIE. Unfortunately, when constructed using standard Rao–Wilton–Glisson basis functions, this Gram matrix is singular [8]. To overcome this problem, the EFIE operator often is split into its singular and hypersingular components and the resulting operator products, safe the square of the *continuous* hypersingular operator which vanishes, are approximated using ad hoc discretization/integration rules [6], [7]. This procedure is computationally expensive—it calls for additional matrix–vector products—and often inaccurate as the square of the *discretized* hypersingular operator typically does not vanish. Moreover, the resulting preconditioners are not multiplicative, and therefore, hard to integrate into existing EFIE MoM codes; in addition, they do not easily apply to open structures [6].

This paper presents a Calderón multiplicative preconditioner (CMP) that is trivially integrated into existing EFIE MoM codes. The proposed CMP is rooted in the div- and quasicurl-conforming basis proposed by Buffa and Christiansen [10] for constructing Calderón preconditioners that avoid the above pitfalls. The purpose and contributions of this paper are twofold: 1) to introduce the Buffa–Christiansen (BC) basis to the computational electromagnetics (CEM) engineering community and 2) to derive transformation rules linking BC and RWG basis on barycentrically refined and standard meshes. Together, the BC basis and the transformation rules derived herein permit the construction of well-conditioned weighted squares of EFIE MoM interaction matrices produced by *standard* RWG codes acting on barycentrically refined meshes. The weighting matrices comprise two sparse and readily computed transformation matrices linking standard RWG spaces on standard and barycentrically refined triangular patch meshes, and one sparse and well-conditioned Gram matrix linking RWG and BC basis functions on a barycentrically refined triangular patch mesh. As an added advantage over existing Calderón preconditioners, the proposed preconditioner not only applies to closed structures, but (with minor modifications) to open ones as well. The BC functions represent a subset of the functions introduced by Wilton and

Chen [11] to discretize integral equations pertinent to the analysis of scattering from penetrable objects. However, the well-conditioned nature of the Gram matrices linking BC functions to (curl-conforming) RWGs is not necessarily ensured by using the functions in [11]. This property, which is key to the development of the CMP, justifies the use of BC over the more generic form in [11].

This paper is organized as follows. Section II presents background material and introduces notation. Section III describes the CMP for closed structures and uniform discretizations. Section IV extends the ideas of Section III to open structures. Section V introduces a modified CMP applicable to nonuniform discretizations. Section VI presents numerical results that demonstrate the effectiveness of the CMP in lowering the condition number of the discretized EFIE operator and the number of iterations required for convergence. Section VII presents our conclusions and avenues for future research.

II. Background

Let Γ and $\hat{\boldsymbol{n}}_{\boldsymbol{r}}$ denote the surface of an orientable PEC object and its outward pointing unit normal at $\boldsymbol{r}$, respectively. Assume that Γ resides in a homogeneous medium with electric permittivity ϵ and magnetic permeability μ, and is illuminated by a time-harmonic electric field $\boldsymbol{E}^i(\boldsymbol{r})$; here and in what follows, a time dependence $e^{-i\omega t}$ is assumed and suppressed. The current density $\boldsymbol{J}(\boldsymbol{r})$ induced on Γ in response to $\boldsymbol{E}^i(\boldsymbol{r})$ produces the scattered field $\boldsymbol{E}^s(\boldsymbol{r})$. The components tangential to Γ of $\boldsymbol{E}^s(\boldsymbol{r})$ cancel those of $\boldsymbol{E}^i(\boldsymbol{r})$, or

$$\hat{\boldsymbol{n}}_{\boldsymbol{r}} \times \boldsymbol{E}^s = \mathcal{T}(\boldsymbol{J}) = -\hat{\boldsymbol{n}}_{\boldsymbol{r}} \times \boldsymbol{E}^i \tag{1}$$

where

$$\mathcal{T}(\boldsymbol{J}) = \mathcal{T}_s(\boldsymbol{J}) + \mathcal{T}_h(\boldsymbol{J}) \tag{2}$$

with

$$\mathcal{T}_s(\boldsymbol{J}) = i\omega\mu\hat{\boldsymbol{n}}_{\boldsymbol{r}} \times \int_\Gamma \frac{e^{-ik|\boldsymbol{r}-\boldsymbol{r}'|}}{4\pi|\boldsymbol{r}-\boldsymbol{r}'|}\boldsymbol{J}(\boldsymbol{r}')\mathrm{d}\boldsymbol{r}' \tag{3}$$

and

$$\mathcal{T}_h(\boldsymbol{J}) = -\frac{1}{i\omega\epsilon}\hat{\boldsymbol{n}}_{\boldsymbol{r}} \times \nabla \int_\Gamma \frac{e^{-ik|\boldsymbol{r}-\boldsymbol{r}'|}}{4\pi|\boldsymbol{r}-\boldsymbol{r}'|}\nabla_s \cdot \boldsymbol{J}(\boldsymbol{r}')\mathrm{d}\boldsymbol{r}' \tag{4}$$

and $k = 2\pi/\lambda = \omega\sqrt{\epsilon\mu}$. To solve EFIE (1) using the MoM, Γ is approximated by a mesh of planar triangles with minimum edge size δ, and $\boldsymbol{J}(\boldsymbol{r})$ is approximated as

$$\boldsymbol{J}(\boldsymbol{r}) \approx \sum_{n=1}^{N} I_n \boldsymbol{f}_n(\boldsymbol{r}) \tag{5}$$

where $\boldsymbol{f}_n(\boldsymbol{r})$, $n = 1, \ldots, N$, are Rao–Wilton–Glisson div-conforming basis functions defined on the mesh's N internal edges as [12] (Fig. 1)

$$\boldsymbol{f}_n(\boldsymbol{r}) = \begin{cases} \dfrac{l_n}{2A_n^+}\rho_n^+, & \boldsymbol{r} \in T_n^+ \\ \dfrac{l_n}{2A_n^-}\rho_n^-, & \boldsymbol{r} \in T_n^- \\ 0, & \text{otherwise.} \end{cases} \tag{6}$$

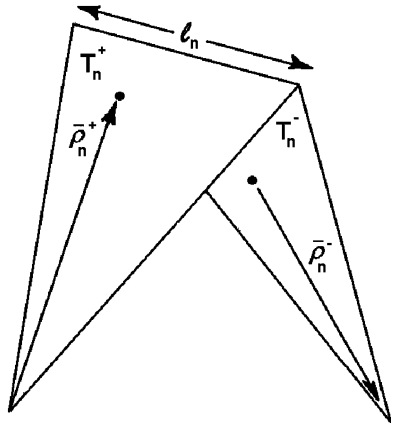

Fig. 1. RWG basis function defined on the edge n; T^+ and T^- indicate the positive charge ($\nabla \cdot \boldsymbol{f}_n > 0$) and negative charge ($\nabla \cdot \boldsymbol{f}_n < 0$) cell, respectively, and l_n denotes the length of the edge.

Henceforth, X_{RWG} denotes the space spanned by these functions. To determine the expansion coefficients I_n, (5) is substituted into (1) and the resulting equation is tested with curl-conforming functions $\hat{\boldsymbol{n}}_{\boldsymbol{r}} \times \boldsymbol{f}_n$ yielding the $N \times N$ EFIE MoM system

$$\bar{\bar{\mathbf{Z}}}\bar{\mathbf{I}} = \bar{\mathbf{V}} \tag{7}$$

where

$$(\bar{\bar{\mathbf{Z}}})_{i,j} = \langle \hat{\boldsymbol{n}}_{\boldsymbol{r}} \times \boldsymbol{f}_i, \mathcal{T}(\boldsymbol{f}_j) \rangle \tag{8}$$

$$(\bar{\mathbf{V}})_i = -\langle \hat{\boldsymbol{n}}_{\boldsymbol{r}} \times \boldsymbol{f}_i, \hat{\boldsymbol{n}}_{\boldsymbol{r}} \times \boldsymbol{E}^i \rangle \tag{9}$$

$$(\bar{\mathbf{I}})_j = I_j. \tag{10}$$

Notwithstanding its appearance, (7) is the standard EFIE MoM system proposed in [12]. For large N, (7) only can be solved iteratively. Unfortunately, $\mathcal{T}$'s singular values accumulate around zero and infinity [5] and the matrix $\bar{\bar{\mathbf{Z}}}$ has a high condition number when $\delta \to 0$.[1] Under these conditions, the iterative solution of (7) converges very slowly [14], [15].

Since the ill-conditioning of $\bar{\bar{\mathbf{Z}}}$ is rooted in the spectral properties of $\mathcal{T}$, the above problem can be mitigated by transforming $\mathcal{T}$ into a more regular operator, e.g., by leveraging the Calderón identity [16]

$$\mathcal{T}^2(\boldsymbol{J}) = -\frac{\boldsymbol{J}}{4} + \mathcal{K}^2(\boldsymbol{J}) \tag{11}$$

where the operator

$$\mathcal{K}(\boldsymbol{J}) = \hat{\boldsymbol{n}}_{\boldsymbol{r}} \times \nabla \times \int_\Gamma \frac{e^{-ik|\boldsymbol{r}-\boldsymbol{r}'|}}{4\pi|\boldsymbol{r}-\boldsymbol{r}'|}\boldsymbol{J}(\boldsymbol{r}')\mathrm{d}\boldsymbol{r}' \tag{12}$$

is compact on smooth surfaces [5]. In other words, $\mathcal{T}^2$ is a second kind operator and its spectrum accumulates at -0.25. Equation (11) suggests that $\mathcal{T}$ "preconditions itself" and that discretization of

$$\mathcal{T}^2(\boldsymbol{J}) = \mathcal{T}(-\hat{\boldsymbol{n}}_{\boldsymbol{r}} \times \boldsymbol{E}^i) \tag{13}$$

[1]The condition number of $\bar{\bar{\mathbf{Z}}}$ is defined as the ratio of $\bar{\bar{\mathbf{Z}}}$'s largest and smallest singular values [13].

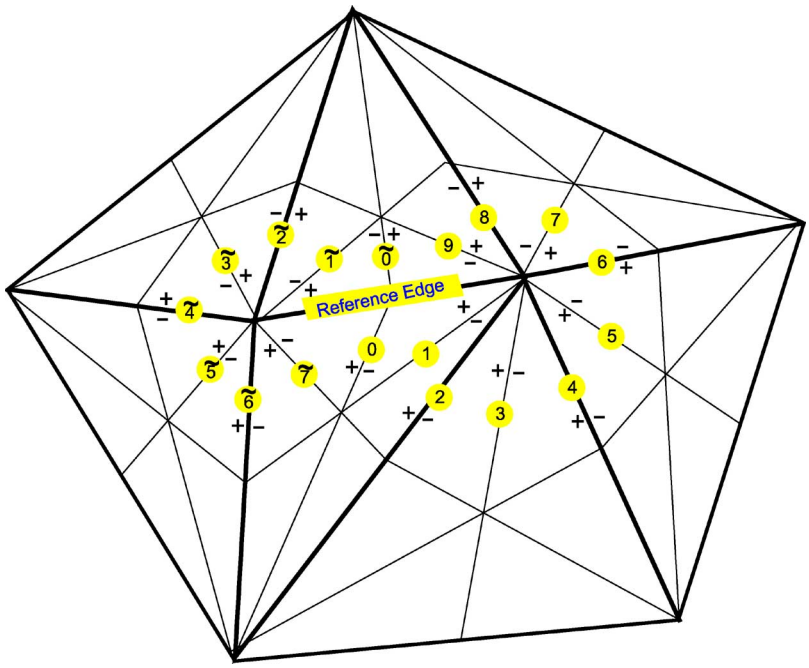

Fig. 2. Barycentric edges used in the definition of the BC basis function associated with the reference edge. A plus/minus sign near the edge denotes a "positive/negative-charge cell" T_n^+ / T_n^- for the barycentric RWG defined on the edge.

leads to well-conditioned EFIE MoM systems independently of δ. Unfortunately, the direct discretization of $\mathcal{T}^2$ is infeasible as $\mathcal{T}(\boldsymbol{f}_n)$ is not available in closed form. That said, a variety of methods that discretize each factor in the product $\mathcal{T}^2$ using ad hoc integration rules and/or operatorial manipulations exists [6], [7], [9]. Unfortunately, none of them can be implemented directly starting from an implementation of (7). In fact, when div- and curl-conforming RWGs are used to discretize the source/testing space of $\mathcal{T}$, the discretization of the operator $\mathcal{T}^2$ would require the inversion of a mixed div- and curl-conforming Gram matrix $\bar{\bar{\mathbf{G}}}_{i,j} = \langle \hat{\boldsymbol{n}}_{\boldsymbol{r}} \times \boldsymbol{f}_i, \boldsymbol{f}_j \rangle$, which is singular. Recent attempts to solve this problem decompose $\mathcal{T}^2(\boldsymbol{J})$ as

$$\mathcal{T}^2(\boldsymbol{J}) = \mathcal{T}_s\mathcal{T}_s(\boldsymbol{J}) + \mathcal{T}_s\mathcal{T}_h(\boldsymbol{J}) + \mathcal{T}_h\mathcal{T}_s(\boldsymbol{J}) + \mathcal{T}_h\mathcal{T}_h(\boldsymbol{J}) \quad (14)$$

and discretize each product—$\mathcal{T}_h\mathcal{T}_h(\boldsymbol{J})$ which vanishes, aside (see below)—with a different technique. This procedure is problematic for the following reasons. First, it increases computational costs as additional matrix–vector products are called for. Second, it introduces additional errors since [discrete $\mathcal{T}_h\mathcal{T}_h(\boldsymbol{J})$] is set to zero even though its discretization consistent with that adopted for the other three products would have dictated [discrete $\mathcal{T}_h\mathcal{T}_h(\boldsymbol{J})] \neq 0$.

Third and most important, it precludes the use of the original $\bar{\bar{\mathbf{Z}}}$ (or a matrix produced by a standard EFIE MoM code). These drawbacks—shared by all Calderón preconditioners developed to date—dramatically compromise these techniques's integrability into existing EFIE solvers and limit their present impact on the CEM state of the art.

III. CMP for Closed Structures

This section presents a discretization of (13) that explicitly uses a weighted square of $\bar{\bar{\mathbf{Z}}}$ defined in (8) on a properly constructed mesh; this matrix can be obtained from any preexisting EFIE code. The weighting matrices required are highly sparse—they only contain $O(N)$ nonzero elements—and can be evaluated from simple, closed-form expressions. The proposed formulation can be trivially integrated into existing frequency domain EFIE solvers and is easily extended to marching on in time-based EFIE solvers [17]. For simplicity, the formulation in this section is restricted to uniformly discretized and closed structures (i.e., the edges in the mesh are approximately of the same length). The preconditioner extension to open structures and to nonuniform discretizations is discussed in Sections IV and V, respectively.

This section is organized as follows. Section III-A outlines the proposed preconditioning strategy. Section III-B proves an important inclusion relationship that permits RWG functions defined on an arbitrary triangular mesh to be expanded in terms of those defined on its barycentric refinement. Section III-C uses this result to obtain simple closed-from expression for all weighting matrices.

A. The Preconditioner

Starting from an arbitrary mesh of planar triangles that discretize Γ—further termed the *initial mesh*—a *barycentric mesh* is obtained by adding the three medians to each triangle (Fig. 2). Note that a set of RWG basis functions $\boldsymbol{f}^b$ can be defined on this barycentric mesh; X^B_{RWG} will denote the space spanned by these functions. The proposed preconditioner adopts a discretization of the dual of the range of $\mathcal{T}$ on the barycentric mesh using the BC div-conforming basis functions [10]; below these basis functions will be denoted $\boldsymbol{f}_{\mathrm{BC}}$ and the space they span will be denoted X_{BC}.

As stated before, the main problem in the discretization of $\mathcal{T}^2$ stems from the need to use div- and curl-conforming

functions to discretize the source/testing space of $\mathcal{T}$ along with the fact that the determinant of the Gram matrix linking curl- and div-conforming RWGs vanishes. The latter is because the space of N div-conforming RWGs contains a subspace of dimension approximately $N/3$ that is nearly orthogonal to the space of curl-conforming RWGs. The BC basis functions (which are fully described in Section III-C2) are defined on the edges of the initial mesh and are linear combinations of div-conforming RWGs defined on the barycentric mesh. These functions are strictly div-conforming (by construction); they also are quasicurl-conforming in that they very much behave like curl-conforming RWGs [Fig. 7(c)]. As a consequence, the Gram matrix linking BC and curl-conforming RWGs is well conditioned because it behaves like the Gram matrix linking curl- and curl-conforming RWGs whose condition number is notoriously low when the discretization is uniform [6]. These insights lead to the following discretization strategy for $\mathcal{T}^2$: the right operator $\mathcal{T}$ is discretized by using div-conforming RWGs $\boldsymbol{f}$ (source) and curl-conforming RWGs $\hat{\boldsymbol{n}}_{\boldsymbol{r}} \times \boldsymbol{f}$ (test), while the left operator is discretized by using div- and quasicurl-conforming BCs $\boldsymbol{f}_{\rm BC}$ (source) and curl- and quasidiv-conforming BCs $\hat{\boldsymbol{n}}_{\boldsymbol{r}} \times \boldsymbol{f}_{\rm BC}$ (test). The inverse Gram matrix between $\hat{\boldsymbol{n}}_{\boldsymbol{r}} \times \boldsymbol{f}$ and $\boldsymbol{f}_{\rm BC}$ links the two discretizations. In other words

$$(\mathcal{T}^2)_{\rm dis} = \bar{\bar{\mathbf{Z}}}_{\rm BC} \bar{\bar{\mathbf{G}}}_m^{-1} \bar{\bar{\mathbf{Z}}} \tag{15}$$

where

$$(\bar{\bar{\mathbf{Z}}})_{i,j} = \langle \hat{\boldsymbol{n}}_{\boldsymbol{r}} \times \boldsymbol{f}_i, \mathcal{T}(\boldsymbol{f}_j) \rangle \tag{16}$$

$$(\bar{\bar{\mathbf{Z}}}_{\rm BC})_{i,j} = \langle \hat{\boldsymbol{n}}_{\boldsymbol{r}} \times \boldsymbol{f}_{{\rm BC}i}, \mathcal{T}(\boldsymbol{f}_{{\rm BC}j}) \rangle \tag{17}$$

and

$$(\bar{\bar{\mathbf{G}}}_m)_{i,j} = \langle \hat{\boldsymbol{n}}_{\boldsymbol{r}} \times \boldsymbol{f}_i, \boldsymbol{f}_{{\rm BC}j} \rangle. \tag{18}$$

The implementation of (15) can be reconducted to the computation of a single impedance matrix $\bar{\bar{\mathbf{Z}}}^b$ defined on the baricentric mesh, computable (and compressible) using standard codes. This is accomplished by using two transformation matrices $\bar{\bar{\mathbf{P}}} \in \mathbb{R}^{N^b \times N}$ and $\bar{\bar{\mathbf{R}}} \in \mathbb{R}^{N^b \times N}$ (to be defined) that express functions in $X_{\rm BC}$ and $X_{\rm RWG}$ as linear combinations of functions in $X^B_{\rm RWG}$, respectively. The former set of coefficients has been derived in [10] and will be reviewed in Section III-C2; the latter set will be derived in Section III-B. Using (15) and defining

$$(\bar{\bar{\mathbf{Z}}}^b)_{i,j} = \left\langle \hat{\boldsymbol{n}}_{\boldsymbol{r}} \times \boldsymbol{f}^b_i, \mathcal{T}\left(\boldsymbol{f}^b_j\right) \right\rangle \tag{19}$$

$$(\bar{\mathbf{V}}^b)_i = -\left\langle \hat{\boldsymbol{n}}_{\boldsymbol{r}} \times \boldsymbol{f}^b_i, \hat{\boldsymbol{n}}_{\boldsymbol{r}} \times \boldsymbol{E}^i \right\rangle \tag{20}$$

$$\bar{\bar{\mathbf{Q}}} = \bar{\bar{\mathbf{P}}} \bar{\bar{\mathbf{G}}}_m^{-1} \bar{\bar{\mathbf{R}}}^T \tag{21}$$

(13) is converted into matrix equation

$$(\bar{\bar{\mathbf{P}}}^T \bar{\bar{\mathbf{Z}}}^b \bar{\bar{\mathbf{Q}}} \bar{\bar{\mathbf{Z}}}^b \bar{\bar{\mathbf{R}}}) \bar{\mathbf{I}} = (\bar{\bar{\mathbf{P}}}^T \bar{\bar{\mathbf{Z}}}^b \bar{\bar{\mathbf{Q}}}) \bar{\mathbf{V}}^b \tag{22}$$

which is the proposed CMP. The vector $\bar{\bar{\mathbf{I}}} \in \mathbb{C}^N$ is the same as that appearing in (7), i.e., it contains expansion coefficients vector for RWGs defined on the *initial* mesh.

Closed-form expressions for the elements of the (transformation and Gram) weighting matrices $\bar{\bar{\mathbf{R}}}$, $\bar{\bar{\mathbf{P}}}$, and $\bar{\bar{\mathbf{Q}}}$ will be obtained in Section III-C. Before describing these matrices, the inclusion of the space $X_{\rm RWG}$ spanned by the RWGs defined on the initial mesh and the space $X^b_{\rm RWG}$ spanned by RWGs on the barycentric mesh will be proven and the coefficients that express functions of the former space as linear combinations of functions of the latter will be obtained.

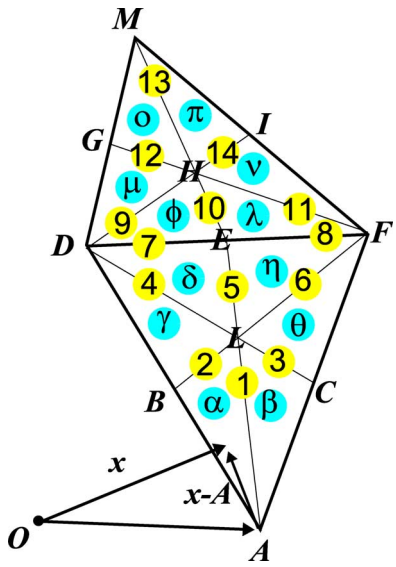

Fig. 3. Edges of the RWGs defined on the barycentric mesh and used in the reconstruction of the RWG defined on the reference edge $(7+8)$ of the initial mesh. A plus/minus sign near the edge denotes a "positive/negative-charge cell" T_n^+ / T_n^- for the barycentric RWG defined on the edge.

B. The $X_{\rm RWG} - X^b_{\rm RWG}$ Inclusion Relationship

Below it will be shown that

$$X_{\rm RWG} \subset X^b_{\rm RWG}. \tag{23}$$

The proof is constructive, that is, the coefficients that realize the mapping from $X^b_{\rm RWG}$ to $X_{\rm RWG}$ will be found explicitly.

Consider an arbitrary RWG function $\boldsymbol{f} \in X_{\rm RWG}$ defined on the initial mesh and the set $\boldsymbol{f}^B_i \in X^b_{\rm RWG}$, $i = 1 \ldots, 14$, of RWGs defined on the barycentric mesh with support *completely included* in that of $\boldsymbol{f}$ (Fig. 3). The function $\boldsymbol{f}$ is expressed as the linear combination

$$\boldsymbol{f} = \sum_{i=1}^{14} c_i \boldsymbol{f}^b_i. \tag{24}$$

Below, the scalars c_i are shown to have simple analytical expressions.

The notation adopted is the following (Fig. 3): cells are indexed with Greek letters; vertices are denoted by capital letters $\boldsymbol{A}, \boldsymbol{B}, \boldsymbol{C}, \boldsymbol{D}, \boldsymbol{E}, \boldsymbol{F}, \boldsymbol{G}, \boldsymbol{H}, \boldsymbol{I}, \boldsymbol{L}, \boldsymbol{M}$ (thought of as position vectors anchored to an arbitrary origin $\boldsymbol{O}$); internal edges are numbered 1 through 14; and "$\boldsymbol{x}$" denotes an arbitrary position vector [referenced with respect to (w.r.t.) to $\boldsymbol{O}$]. Edge lengths in the barycentric mesh are denoted l_i, $i = 1, \ldots, 14$, and cell areas in the barycentric mesh are denoted A_q, $q = \alpha, \beta, \ldots, \pi$. The orientation of the barycentric RWGs is defined in Fig. 3 (a $+/-$

near an edge defines a "positive/negative-charge cell" T^+/T^- for the associated RWG); the RWG $\boldsymbol{f}$ defined on the initial mesh is oriented so that its $+$ cell is the union of cells α, β, γ, δ, η, and θ. Finally, define

$$A^+ = A_\alpha + A_\beta + A_\gamma + A_\delta + A_\eta + A_\theta = 6A_\alpha \quad (25)$$

$$A^- = A_\phi + A_\lambda + A_\mu + A_\nu + A_o + A_\pi = 6A_\phi \quad (26)$$

$$l = l_7 + l_8 = 2l_7. \quad (27)$$

The coefficients c_i, $i = 1, \ldots, 14$, will be determined by leveraging the polynomial equivalence principle [18] enforced on each cell included in the support of $\boldsymbol{f}$.

1) Cell α: From (6), the equivalence equation in cell α reads

$$-\frac{\boldsymbol{x}-\boldsymbol{A}}{A_\alpha} l_2 c_2 + \frac{\boldsymbol{x}-\boldsymbol{B}}{A_\alpha} l_1 c_1 = \frac{\boldsymbol{x}-\boldsymbol{A}}{A^+} l \qquad \forall \boldsymbol{x} \in \alpha. \quad (28)$$

Taking $\boldsymbol{x} = \boldsymbol{A}$, it follows that

$$c_1 = 0. \quad (29)$$

Because $A^+ = 6A_\alpha$

$$c_2 = -\frac{l}{A^+}\frac{A_\alpha}{l_2} = -\frac{l}{6l_2} \quad (30)$$

and from symmetry, it follows that

$$c_3 = \frac{l}{6l_3} \quad c_{13} = 0 \quad c_{12} = -\frac{l}{6l_{12}} \quad c_{14} = \frac{l}{6l_{14}}. \quad (31)$$

2) Cell γ: The equivalence equation in the cell γ reads

$$\frac{\boldsymbol{x}-\boldsymbol{D}}{A_\gamma} l_2 c_2 - \frac{\boldsymbol{x}-\boldsymbol{B}}{A_\gamma} l_4 c_4 = \frac{\boldsymbol{x}-\boldsymbol{A}}{A^+} l \qquad \forall \boldsymbol{x} \in \gamma. \quad (32)$$

Enforcing equality of the linear terms yields

$$l_2 A^+ c_2 - l_4 A^+ c_4 = l A_\gamma \quad (33)$$

so that

$$c_4 = -\frac{l}{A^+}\frac{A_\alpha + A_\gamma}{l_4} = -\frac{l}{3l_4}. \quad (34)$$

This value has to satisfy the equality of the constant terms

$$-\boldsymbol{D} l A^+ c_2 + \boldsymbol{B} l_4 A^+ c_4 = -\boldsymbol{A} l A_\gamma. \quad (35)$$

Substituting (30) and (34) into (35) yields

$$\boldsymbol{A} - \boldsymbol{B} = \boldsymbol{B} - \boldsymbol{D} \quad (36)$$

which is satisfied because the two vectors $(\boldsymbol{A}-\boldsymbol{B})$ and $(\boldsymbol{B}-\boldsymbol{D})$ are aligned and equal (due to the definition of median). From

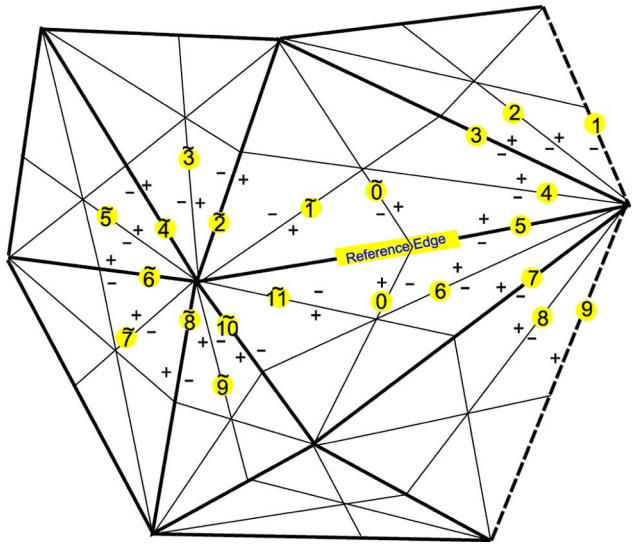

Fig. 4. Barycentric edges used in the definition of the BC function when the reference edge has one vertex on the boundary. The hatched line denotes the boundary. A plus/minus sign near the edge denotes a "positive/negative-charge cell" T_n^+/T_n^- for the barycentric RWG defined on the edge. Note the presence of two half RWGs (labeled 1 and 9) defined on two boundary barycentric edges. A plus sign near a boundary barycentric edge indicates that the corresponding half-RWG follows the definition in (57); a minus sign indicates that the function defined in (57) has to be multiplied by -1.

symmetry, it follows that

$$c_6 = \frac{l}{3l_6} \quad c_9 = -\frac{l}{3l_9} \quad c_{11} = \frac{l}{3l_{11}}. \quad (37)$$

3) Cells δ, η, λ, and ϕ: The equalities in these four cells give rise to the system

$$\begin{cases} -\frac{\boldsymbol{x}-\boldsymbol{H}}{A_\phi} l_7 c_7 + \frac{\boldsymbol{x}-\boldsymbol{D}}{A_\phi} l_{10} c_{10} - \frac{\boldsymbol{x}-\boldsymbol{E}}{A_\phi} l_9 c_9 = -\frac{\boldsymbol{x}-\boldsymbol{M}}{A^-} l & \forall \boldsymbol{x} \in \phi \\ \frac{\boldsymbol{x}-\boldsymbol{F}}{A_\eta} l_5 c_5 - \frac{\boldsymbol{x}-\boldsymbol{E}}{A_\eta} l_6 c_6 + \frac{\boldsymbol{x}-\boldsymbol{L}}{A_\eta} l_8 c_8 = \frac{\boldsymbol{x}-\boldsymbol{A}}{A^+} l & \forall \boldsymbol{x} \in \eta \\ \frac{\boldsymbol{x}-\boldsymbol{E}}{A_\delta} l_4 c_4 - \frac{\boldsymbol{x}-\boldsymbol{D}}{A_\delta} l_5 c_5 + \frac{\boldsymbol{x}-\boldsymbol{L}}{A_\delta} l_7 c_7 = \frac{\boldsymbol{x}-\boldsymbol{A}}{A^+} l & \forall \boldsymbol{x} \in \delta \\ -\frac{\boldsymbol{x}-\boldsymbol{H}}{A_\lambda} l_8 c_8 - \frac{\boldsymbol{x}-\boldsymbol{F}}{A_\lambda} l_{10} c_{10} + \frac{\boldsymbol{x}-\boldsymbol{E}}{A_\lambda} l_{11} c_{11} = -\frac{\boldsymbol{x}-\boldsymbol{M}}{A^-} l & \forall \boldsymbol{x} \in \lambda. \end{cases} \quad (38)$$

The equality of the linear terms yields to the system

$$\begin{cases} l_7 c_7 - l_5 c_5 = l/2 \\ l_7 c_7 - l_{10} c_{10} = l/2 \\ l_5 c_5 + l_8 c_8 = l/2 \\ l_8 c_8 + l_{10} c_{10} = l/2 \end{cases} \quad (39)$$

which has solutions

$$c_5 = 0 \quad c_7 = 1 \quad c_8 = 1 \quad c_{10} = 0. \quad (40)$$

The condition arising from the equality of the constant terms, obtained by substituting the values in (40), reads (after some manipulations)

$$\begin{cases} \boldsymbol{E} - \boldsymbol{H} = (\boldsymbol{M} - \boldsymbol{E})/3 \\ (\boldsymbol{E} - \boldsymbol{A})/3 = (\boldsymbol{L} - \boldsymbol{A})/2 \\ \boldsymbol{E} - \boldsymbol{L} = (\boldsymbol{E} - \boldsymbol{A})/3 \\ (\boldsymbol{E} - \boldsymbol{M})/3 = (\boldsymbol{H} - \boldsymbol{M})/2 \end{cases} \quad (41)$$

TABLE I
SPHERE: CENTRAL PROCESSING UNIT (CPU) TIMES REQUIRED FOR THE SOLUTION OF THE DIAGONAL- AND CMP-PRECONDITIONED EFIE MOM SYSTEMS

δ	Number RWGs on the standard mesh	Standard EFIE solution time (s)	CMP solution time (s)
0.02λ	1140	26.98	11.26
0.015λ	10062	495.22	59.89
0.00375λ	100596	21699.2	799.40
0.00115λ	520257	-	1868.48

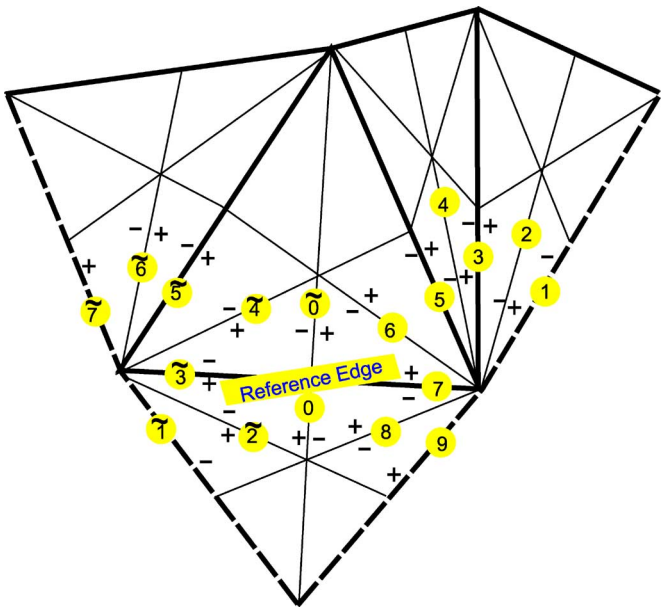

Fig. 5. Barycentric edges used in the definition of the BC function when the reference edge has two vertices on the boundary. The hatched line denotes the boundary. A plus/minus sign near the edge denotes a "positive/negative-charge cell" T_n^+/T_n^- for the barycentric RWG defined on the edge. Note the presence of four half RWGs (labeled 1, 9, $\bar{1}, \bar{7}$) defined on four boundary barycentric edges. A plus sign near a boundary barycentric edge indicates that the corresponding half-RWG follows the definition in (57); a minus sign indicates that the function defined in (57) has to be multiplied by -1.

which is always satisfied in the barycentric mesh. In conclusion

$$\begin{aligned}\boldsymbol{f}(\boldsymbol{x}) = &-\frac{l}{6l_2}\boldsymbol{f}_2(\boldsymbol{x}) + \frac{l}{6l_3}\boldsymbol{f}_3(\boldsymbol{x}) - \frac{l}{3l_4}\boldsymbol{f}_4(\boldsymbol{x}) + \frac{l}{3l_6}\boldsymbol{f}_6(\boldsymbol{x}) \\ &+ \boldsymbol{f}_7(\boldsymbol{x}) + \boldsymbol{f}_8(\boldsymbol{x}) - \frac{l}{3l_9}\boldsymbol{f}_9(\boldsymbol{x}) + \frac{l}{3l_{11}}\boldsymbol{f}_{11}(\boldsymbol{x}) \\ &- \frac{l}{6l_{12}}\boldsymbol{f}_{12}(\boldsymbol{x}) + \frac{l}{6l_{14}}\boldsymbol{f}_{14}(\boldsymbol{x}) \qquad \forall \boldsymbol{x} \in \Gamma. \end{aligned} \tag{42}$$

This concludes the proof.

An alternative method to obtain the coefficients in (42) consists of equating, on each edge of each barycentric RWG function $f_i(\boldsymbol{r})$, $i = 1, \ldots, 14$, the normal component of the RWG on the initial mesh $f(\boldsymbol{r})$ to that of (24). This follows from the fact that the degrees of freedom of the RWG functions are completely exhausted by the functions' normal component values evaluated on the functions' edges [10].

The validity of (23) enables the construction of the previously escribed preconditioner with weighting matrices detailed in Section III-C.

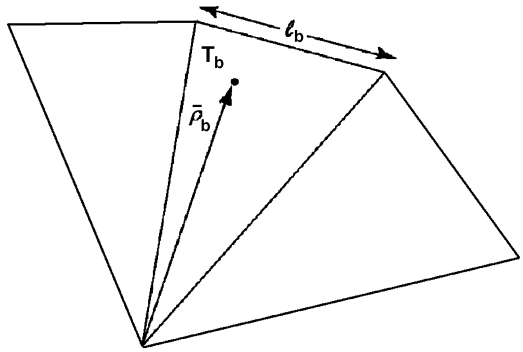

Fig. 6. Half-RWG function defined on the cell T_b of area A_b and associated with the boundary edge b of length l_b.

C. Weighting Matrices

This section describes the matrices $\bar{\bar{\mathbf{R}}}$, $\bar{\bar{\mathbf{P}}}$, and $\bar{\bar{\mathbf{Q}}}$ appearing in (22).

1) Matrix $\bar{\bar{\mathbf{R}}}$: As stated in Section III-A, matrix $\bar{\bar{\mathbf{R}}}$ maps space X_{RWG} onto space X^b_{RWG}. $\bar{\bar{\mathbf{R}}}$'s column indices point to RWGs on the initial mesh, while $\bar{\bar{\mathbf{R}}}$'s row indices denote RWGs on the barycentric one. It follows that a column of $\bar{\bar{\mathbf{R}}}$ contains fourteen elements, viz., the coefficients in (42). Note that $\bar{\bar{\mathbf{R}}}$ contains $O(N)$ elements and can be applied to a vector in $O(N)$ operations.

2) Matrix $\bar{\bar{\mathbf{P}}}$: The matrix $\bar{\bar{\mathbf{P}}}$ realizes the mapping between div-conforming RWGs defined on the barycentric mesh ($\boldsymbol{f} \in X^b_{\mathrm{RWG}}$) and the div- and quasicurl-conforming BC functions. The latter functions are linear combinations of div-conforming barycentric RWGs in X^b_{RWG}, but are associated with edges of the initial mesh (so that in number they equal the number of RWGs on the initial mesh). The BC are basis functions quasi-curl-conforming in the sense that the Gram matrix linking the BC basis functions and the curl-conforming RWGs defined on the initial mesh ($\hat{\boldsymbol{n}}_{\boldsymbol{r}} \times \boldsymbol{f}$, with $\boldsymbol{f} \in X_{\mathrm{RWG}}$) is well conditioned [10]. The coefficients that express the BC functions as linear combinations of RWGs on the barycentric mesh have been obtained in [10]; they will be reviewed here for the sake of completeness.

One BC function is associated with each edge of the initial mesh (the "reference edge" Fig. 2; below, the conventions of Fig. 3 are reused). Assume an orientation for the reference edge, i.e., define the "right" and the "left" vertices of the edge (note that since in this section the structure is assumed closed, both these vertices are internal to the mesh). Denote by N_c the number of cells of the initial mesh that have the "right" vertex among their vertices; in Fig. 2, $N_c = 5$. Similarly define $\tilde{N}_c$ for the "left" vertex; in Fig. 2, $\tilde{N}_c = 4$. Label the barycentric edges

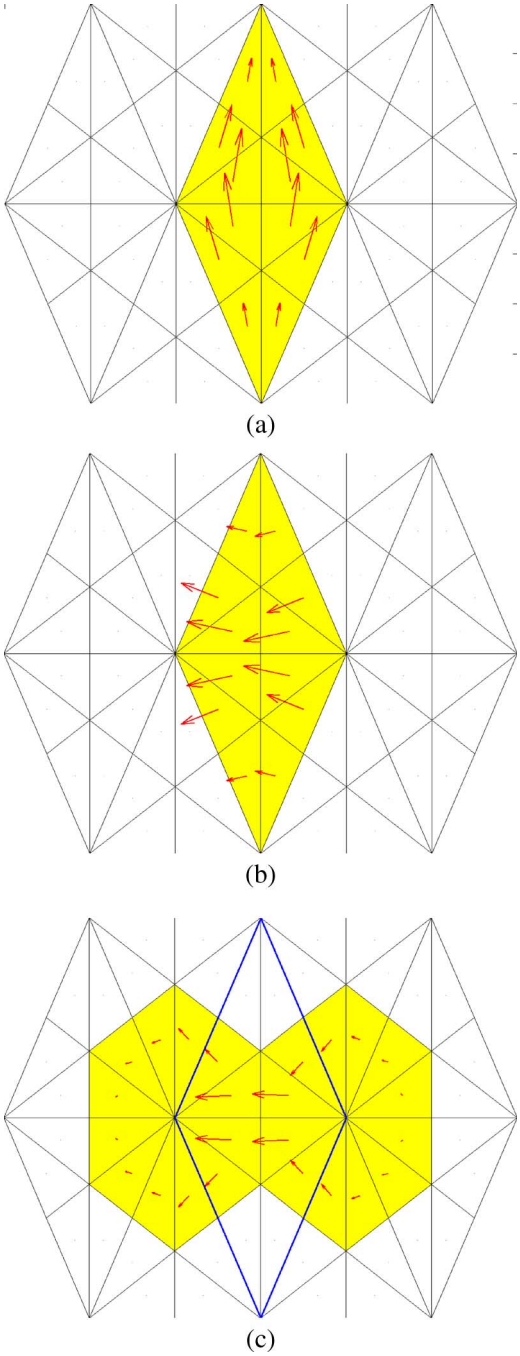

Fig. 7. (a) RWG div-conforming basis function ($\boldsymbol{f}$). (b) RWG curl-conforming basis function ($\hat{\boldsymbol{n}}_{\boldsymbol{r}} \times \boldsymbol{f}$). (c) BC quasicurl-conforming basis function (linear combination of div-conforming RWGs defined on the barycentric mesh).

as in Fig. 2: $1, 2, \ldots, 2N_c - 1$ on the right and $\tilde{1}, \tilde{2}, \ldots, 2\tilde{N}_c - 1$ on the left. The two barycentric RWGs in the middle will be labeled 0 and $\tilde{0}$ (Fig. 2). The coefficients of the rightmost RWGs are

$$c_i = \frac{N_c - i}{2l_i N_c}, \qquad i = 1, \ldots, 2N_c - 1 \tag{43}$$

while those for the leftmost RWGs are

$$c_{\tilde{i}} = -\frac{\tilde{N}_c - \tilde{i}}{2l_{\tilde{i}}\tilde{N}_c}, \qquad i = 1, \ldots, 2\tilde{N}_c - 1. \tag{44}$$

The RWGs 0 and $\tilde{0}$ have coefficients $1/2l_0$ and $-1/2l_{\tilde{0}}$, respectively.

In the example of Fig. 2

$$\begin{aligned} &c_0 = \frac{1}{2l_0} \quad c_1 = \frac{4}{10l_1} \quad c_2 = \frac{3}{10l_2} \quad c_3 = \frac{2}{10l_3} \quad c_4 = \frac{1}{10l_4} \\ &c_5 = 0 \quad c_6 = -\frac{1}{10l_6} \quad c_7 = -\frac{2}{10l_7} \quad c_8 = -\frac{3}{10l_8} \\ &c_9 = -\frac{4}{10l_9} \quad c_{\tilde{0}} = -\frac{1}{2l_{\tilde{0}}} \quad c_{\tilde{1}} = -\frac{3}{8l_{\tilde{1}}} \quad c_{\tilde{2}} = -\frac{2}{8l_{\tilde{2}}} \\ &c_{\tilde{3}} = -\frac{1}{8l_{\tilde{3}}} \quad c_{\tilde{4}} = 0 \quad c_{\tilde{5}} = \frac{1}{8l_{\tilde{5}}} \quad c_{\tilde{6}} = \frac{2}{8l_{\tilde{6}}} \quad c_{\tilde{7}} = \frac{3}{8l_{\tilde{7}}}. \end{aligned} \tag{45}$$

Column indices of the matrix $\bar{\bar{\mathbf{P}}}$ point to BC functions defined on the edges of the initial mesh, while its row indices denote RWGs on the barycentrically refined mesh. Thus, a column of $\bar{\bar{\mathbf{P}}}$ contains the coefficients in (43) and (44). Note that, similar to $\bar{\bar{\mathbf{R}}}$, $\bar{\bar{\mathbf{P}}}$ also can be applied to a vector in $O(N)$ operations.

Consider the three BC basis functions $\boldsymbol{f}_{\mathrm{BC}i}$, $i = 1 \ldots 3$, defined by the three reference edges of a cell of the standard mesh and oriented counterclockwise. From the definition of the coefficients in (45), it is easy to see that the function

$$\boldsymbol{f}_s = \sum_{i=1}^{3} \boldsymbol{f}_{\mathrm{BC}i} \tag{46}$$

is solenoidal, i.e., $\nabla_s \cdot \boldsymbol{f}_s = 0$. Note that the function $\boldsymbol{f}_s$ is defined in the way the (nonsolenoidal) "star" basis functions are defined for standard RWGs [19]. In other words, the space of the div-conforming BC basis functions has a solenoidal subspace associated with the cells of the mesh. This situation is dual with respect to the standard div-conforming RWG space that has a solenoidal subspace associated with the nodes of the mesh (via the "loop" basis functions [19]). As detailed in [20], this property enables the aforementioned cancellation of the square of the discretized hypersingular operator.

3) Matrix $\bar{\bar{\mathbf{Q}}}$: The matrix $\bar{\bar{\mathbf{Q}}}$ maps the space of the curl-conforming RWGs (the dual of the range of $\mathcal{T}$) into the space of the div-conforming RWGs X^b_{RWG} (the domain of $\mathcal{T}$). From the definition in (18), it is easy to see that

$$\bar{\bar{\mathbf{G}}}_m = (\bar{\bar{\mathbf{R}}}^T \bar{\bar{\mathbf{G}}} \bar{\bar{\mathbf{P}}}) \tag{47}$$

where $\bar{\bar{\mathbf{G}}} \in \mathbb{R}^{N^b \times N^b}$ is the mixed Gram matrix linking div- and curl-conforming RWGs defined on the barycentric mesh

$$\bar{\bar{\mathbf{G}}}_{i,j} = \int_{\Gamma} \hat{\boldsymbol{n}}_{\boldsymbol{r}} \times \boldsymbol{f}_i^b(\boldsymbol{r}) \cdot \boldsymbol{f}_i^b(\boldsymbol{r}) \mathrm{d}\boldsymbol{r}. \tag{48}$$

Consequently

$$\bar{\bar{\mathbf{Q}}} = \bar{\bar{\mathbf{P}}} (\bar{\bar{\mathbf{R}}}^T \bar{\bar{\mathbf{G}}} \bar{\bar{\mathbf{P}}})^{-1} \bar{\bar{\mathbf{R}}}^T. \tag{49}$$

The integral in (48) can be computed analytically and $\bar{\bar{\mathbf{G}}}$ contains $O(N)$ elements. The inversion in (49) is never carried out

explicitly; rather, the required matrix–vector product is effected via iterative solution of the system

$$(\bar{\bar{\mathbf{R}}}^T \bar{\bar{\mathbf{G}}} \bar{\bar{\mathbf{P}}})\bar{\mathbf{x}} = \bar{\mathbf{y}} \tag{50}$$

which can be effected in $O(N)$ operations, since $\bar{\bar{\mathbf{P}}}$, $\bar{\bar{\mathbf{G}}}$, and $\bar{\bar{\mathbf{R}}}$ are sparse and the condition number (and so the convergence rate of the iterative solver) of the Gram matrix $\bar{\bar{\mathbf{G}}}_m$ is independent of the number of unknowns [10] and is low for uniform discretizations (simple modifications are required for the treatment of nonuniform discretizations; see Section V). In other words, the matrix $\bar{\bar{\mathbf{Q}}}$ can be applied to a vector in $O(N)$ operations.

D. Computational Cost

The computational cost of solving the preconditioned (22) is that of multiplying the matrix in the left-hand side of (22) times the number of iterations. As mentioned previously, the cost of multiplying $\bar{\bar{\mathbf{R}}}$, $\bar{\bar{\mathbf{P}}}$, and $\bar{\bar{\mathbf{Q}}}$ by a vector scales as $O(N)$. Using the multilevel fast multipole method [2], the cost of multiplying $\bar{\bar{\mathbf{Z}}}^b$ by a vector scales as $C_Z + O(N)$ where C_Z is the cost of multiplying the initial mesh impedance matrix $\bar{\bar{\mathbf{Z}}}$ in (7) by a vector. Indeed, even though the dimension of $\bar{\bar{\mathbf{Z}}}^b$ is greater than that of $\bar{\bar{\mathbf{Z}}}$ by a factor 6, the additional degrees of freedom introduced in the barycentric mesh do not change the number of multipoles required for field expansion compared to that used when multiplying $\bar{\bar{\mathbf{Z}}}$. For this reason, the cost of multiplying $\bar{\bar{\mathbf{Z}}}^b$ increases only by an *additive* linear term. It follows that the overall computational cost of solving (22) is

$$C_{\mathrm{TOT}}^{\mathrm{CMP}} = N_{it}^{\mathrm{CMP}} \left(2C_Z + O(N)\right) \tag{51}$$

with N_{it}^{CMP} being the number of iterations necessary to achieve the convergence using the CMP. This cost should be compared to that of solving the standard system (7), viz.,

$$C_{\mathrm{TOT}} = N_{it} C_Z \tag{52}$$

where N_{it} is the number of iterations necessary to achieve the convergence without using the CMP. Because $N_{it}^{\mathrm{CMP}} \ll N_{it}$, it follows that $C_{\mathrm{TOT}} \gg C_{\mathrm{TOT}}^{\mathrm{CMP}}$ justifying the use of the CMP.

IV. CMP for Open Structures

This section extends the formulation of Section III to open Γ. This is possible because, although (11) is valid for closed Γ only, the decomposition (14) and the condition $\mathcal{T}_h^2 = 0$ hold true for both open and closed structures.

Section III-A applies to open Γ without modification. The sole difference between open and closed Γ arises in the definition of the BC functions. The proper definition of the BC functions and construction of the $\bar{\bar{\mathbf{P}}}$ matrix for open Γ is discussed first. Ramifications on the construction of the $\bar{\bar{\mathbf{Z}}}^b$, $\bar{\bar{\mathbf{R}}}$, and $\bar{\bar{\mathbf{Q}}}$ matrices are discussed thereafter.

As is customary, for open Γ, RWG basis are only associated with internal initial mesh edges; no degrees of freedom in the form of nondivergence-conforming half-RWG functions are associated with initial mesh boundary edges. The same holds true for the BC functions; it follows that for open Γ the number of RWG functions continues to equal the number of BC functions. Moreover, the construction of BC functions for edges having no node in common with the Γ's boundary proceeds as explained in Section III-C. It is clear that the definition of the BC basis functions in Section III-C cannot apply to BC functions for edges sharing one or two vertices with Γ's boundary. For such edges, the BC functions need to be redefined. Contrary to RWG functions on open Γ, these BC functions do incorporate half-barycentric-RWGs associated with the barycentric mesh boundary edges. The coefficients of the barycentric full- and half-RWGs will be defined so as to ensure that, even in the presence of the boundary, the BC basis functions still give rise to solenoidal functions when linearly combined around a cell as in (46). As stated previously, this condition is necessary to ensure the cancellation of the square of the discretized hypersingular operator.

When the reference edge of a BC function incorporates one boundary vertex, then assume the edge is oriented so that the "right" vertex is on the boundary (Fig. 4). Let N_c denote the number of initial mesh cells that incorporate the right vertex; in Fig. 4, $N_c = 4$. Label the barycentric mesh edges incorporating the right vertex 1 through $2N_c + 1$, counterclockwise from the upper barycentric mesh boundary edge to the lower one; the two boundary edges are included in the labeling because two half-RWGs are associated with them. Let N_{ref} denote the edge of the barycentric mesh that coincides with the right half of the reference edge; in Fig. 4, $N_{\mathrm{ref}} = 5$. Let $\tilde{N}_c$ denote the number of cells of the initial mesh that incorporate the left vertex; in Fig. 4, $\tilde{N}_c = 6$. Label the edges of the barycentric mesh incorporating the left vertex $\tilde{1}$ through $2\tilde{N}_c + 1$, counterclockwise from the barycentric mesh edge just above the reference edge to the one just below. The two barycentric RWGs in the middle are labeled 0 and $\tilde{0}$ (Fig. 4). The BC function associated with the reference edge comprises barycentric RWGs with coefficients

$$\begin{aligned}
c_i &= \begin{cases} \dfrac{1 - N_c}{l_i N_c}, & i < N_{\mathrm{ref}} \\ \dfrac{2 - N_c}{2 l_i N_c}, & i = N_{\mathrm{ref}} \\ \dfrac{1}{l_i N_c}, & i > N_{\mathrm{ref}} \end{cases}, \qquad i = 1, \ldots, 2N_c + 1 \\
c_{\tilde{i}} &= -\frac{\tilde{N}_c - \tilde{i}}{2 l_{\tilde{i}} \tilde{N}_c}, \qquad i = 1, \ldots, 2\tilde{N}_c - 1 \\
c_0 &= \frac{1}{2 l_0} \\
c_{\tilde{0}} &= -\frac{1}{2 l_{\tilde{0}}}.
\end{aligned} \tag{53}$$

In the example of Fig. 4

$$c_0 = \frac{1}{2l_0} \quad c_1 = -\frac{3}{4l_1} \quad c_2 = -\frac{3}{4l_2} \quad c_3 = -\frac{3}{4l_3}$$
$$c_4 = -\frac{3}{4l_4} \quad c_5 = -\frac{1}{4l_5}$$

$$c_6 = \frac{1}{4l_6} \quad c_7 = \frac{1}{4l_7} \quad c_8 = \frac{1}{4l_8} \quad c_9 = \frac{1}{4l_9}$$
$$c_{\tilde{0}} = -\frac{1}{2l_{\tilde{0}}} \quad c_{\tilde{1}} = -\frac{5}{12l_{\tilde{1}}} \quad c_{\tilde{2}} = -\frac{4}{12l_{\tilde{2}}} \quad c_{\tilde{3}} = -\frac{3}{12l_{\tilde{3}}}$$
$$c_{\tilde{4}} = -\frac{2}{12l_{\tilde{4}}} \quad c_{\tilde{5}} = -\frac{1}{12l_{\tilde{5}}} \quad c_{\tilde{6}} = 0 \quad c_{\tilde{7}} = \frac{1}{12l_{\tilde{7}}}$$
$$c_{\tilde{8}} = \frac{2}{12l_{\tilde{8}}} \quad c_{\tilde{9}} = \frac{3}{12l_{\tilde{9}}} \quad c_{\tilde{1}\tilde{0}} = \frac{4}{12l_{\tilde{1}\tilde{0}}} \quad c_{\tilde{1}\tilde{1}} = \frac{5}{12l_{\tilde{1}\tilde{1}}}. \quad (54)$$

When the reference edge of a BC function incorporates two boundary vertices, let N_c ($\tilde{N}_c$) denote the number of initial mesh cells that incorporate its right (left) vertex; in Fig. 5, $N_c = 4$ ($\tilde{N}_c = 3$). Label the barycentric mesh edges that incorporate the right (left) vertex 1 through $2N_c+1$ ($2\tilde{N}_c+1$), counterclockwise from one boundary edge to the other; the two boundary edges are included because two half-barycentric mesh RWGs are associated with them. Let $N_{\rm ref}$ ($\tilde{N}_{\rm ref}$) denote the edge of the barycentric mesh that coincides with the right (left) half of the reference edge; in Fig. 5, $N_{\rm ref} = 7$ ($\tilde{N}_{\rm ref} = \tilde{3}$). The two barycentric RWGs in the center are labeled 0 and $\tilde{0}$ (Fig. 5). The BC function associated with the reference edge comprises barycentric RWGs with coefficients

$$c_i = \begin{cases} \dfrac{1-N_c}{l_i N_c}, & i < N_{\rm ref} \\ \dfrac{2-N_c}{2l_i N_c}, & i = N_{\rm ref}\,, \\ \dfrac{1}{l_i N_c}, & i > N_{\rm ref} \end{cases} \qquad i = 1, \ldots, 2N_c+1$$

$$c_{\tilde{i}} = \begin{cases} -\dfrac{1-\tilde{N}_c}{l_{\tilde{i}}}\tilde{N}_c, & \tilde{i} < \tilde{N}_{\rm ref} \\ -\dfrac{2-\tilde{N}_c}{2l_{\tilde{i}}}\tilde{N}_c, & \tilde{i} = \tilde{N}_{\rm ref}\,, \\ -\dfrac{1}{l_{\tilde{i}}}\tilde{N}_c, & \tilde{i} > \tilde{N}_{\rm ref} \end{cases} \qquad \tilde{i} = 1, \ldots, 2\tilde{N}_c+1$$

$$c_0 = \frac{1}{2l_0}$$
$$c_{\tilde{0}} = -\frac{1}{2l_{\tilde{0}}}. \quad (55)$$

In the example of Fig. 5

$$c_0 = \frac{1}{2l_0} \quad c_1 = -\frac{3}{4l_1} \quad c_2 = -\frac{3}{4l_2} \quad c_3 = -\frac{3}{4l_3}$$
$$c_4 = -\frac{3}{4l_4} \quad c_5 = -\frac{3}{4l_5} \quad c_6 = -\frac{3}{4l_6} \quad c_7 = -\frac{1}{4l_7}$$
$$c_8 = \frac{1}{4l_8} \quad c_9 = \frac{1}{4l_9} \quad c_{\tilde{0}} = -\frac{1}{2l_{\tilde{0}}} \quad c_{\tilde{1}} = \frac{2}{3l_{\tilde{1}}} \quad c_{\tilde{2}} = \frac{2}{3l_{\tilde{2}}}$$
$$c_{\tilde{3}} = \frac{1}{6l_{\tilde{3}}} \quad c_{\tilde{4}} = -\frac{1}{3l_{\tilde{4}}} \quad c_{\tilde{5}} = -\frac{1}{3l_{\tilde{5}}} \quad c_{\tilde{6}} = -\frac{1}{3l_{\tilde{6}}}$$
$$c_{\tilde{7}} = -\frac{1}{3l_{\tilde{7}}}. \quad (56)$$

The half-RWG functions alluded to before are defined as (Fig. 6)

$$\boldsymbol{f}_b^{half}(\boldsymbol{r}) = \begin{cases} \dfrac{l_b}{2A_b}\rho_b, & \boldsymbol{r} \in T_b \\ 0, & \text{otherwise.} \end{cases} \quad (57)$$

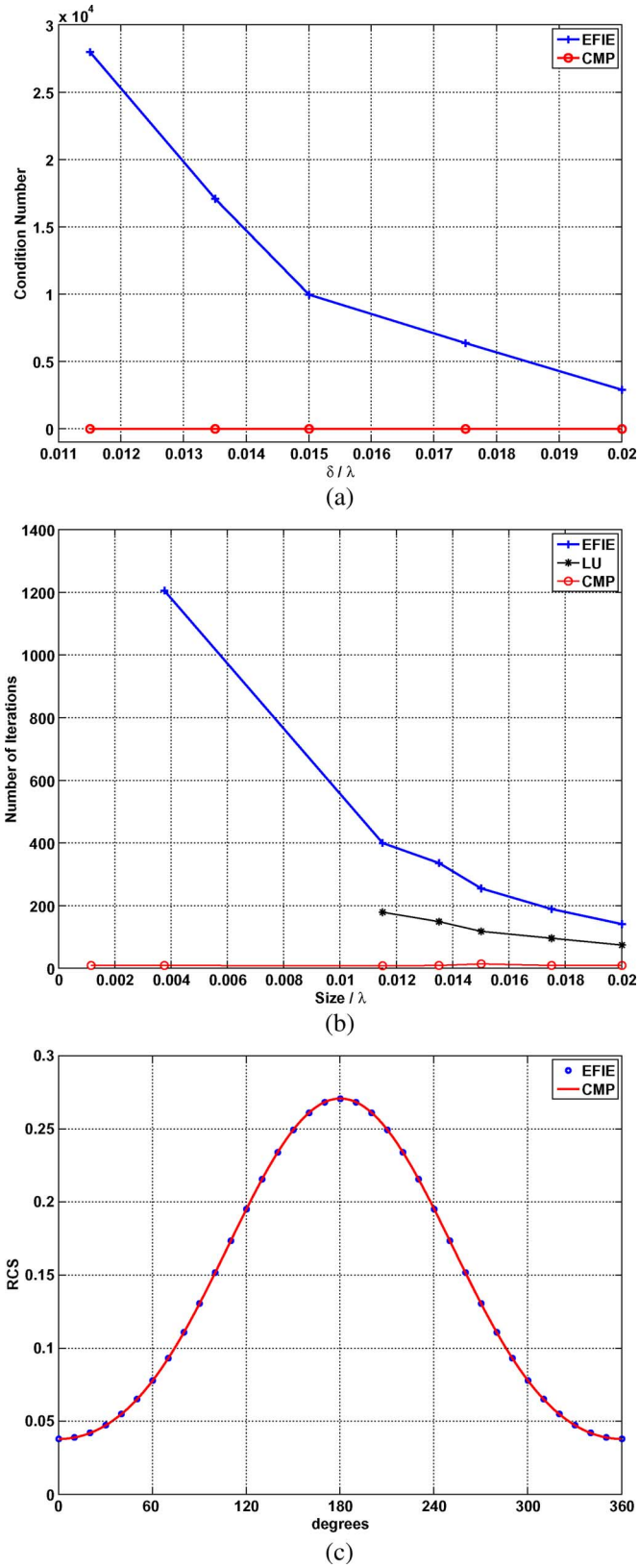

Fig. 8. Analysis of scattering from a sphere. (a) Condition numbers of the diagonal- and CMP-preconditioned EFIE MoM matrices versus δ/λ. (b) Number of iterations required for the relative residual error of the diagonal-, incomplete LU-, and CMP-preconditioned EFIE MoM systems' solutions to reach 10^{-6} versus δ/λ. (c) Comparison of the RCS obtained by solving the diagonal-preconditioned and CMP-preconditioned EFIE MoM systems at $\delta = 0.00375\lambda$.

As the redefined BC functions incorporate half-RWGs on the barycentric mesh, matrix $\bar{\bar{\mathbf{Z}}}^b$ needs to account for them; the

TABLE II
PLATE: CPU TIMES REQUIRED FOR THE SOLUTION OF THE CMP- AND DIAGONAL-PRECONDITIONED EFIE MOM SYSTEMS

δ	Number RWGs on the standard mesh	Standard EFIE solution time (s)	CMP solution time (s)
0.0012λ	13250	502.92	275.82
0.0009λ	20084	605.25	252.89
0.0007λ	34006	725.59	212.54
0.0005λ	61117	1707.42	341.56
0.0003λ	137492	4218.25	602.67
0.0002λ	550930	11431.22	1638.28

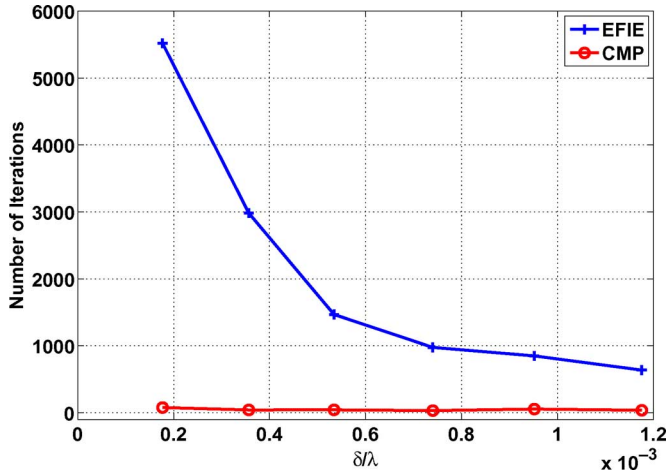

Fig. 9. Analysis of scattering from a plate. Number of iterations required for the relative residual error of the EFIE MoM and preconditioned EFIE MoM systems' solutions to reach 10^{-6} versus δ/λ.

dimension of $\bar{\bar{\mathbf{Z}}}^b$ thus equals the total number of barycentric mesh edges (including the boundary edges). In the open structure case, the CMP (22) remains formally the same. The $\bar{\bar{\mathbf{R}}}$ and $\bar{\bar{\mathbf{Q}}}$ matrices remain defined as in the closed structure case. Because there are no half-RWGs associated with the initial mesh, and because every RWG defined on an internal edge of the initial mesh can be written as a linear combination of barycentric full-RWGs only (no barycentric half-RWGs are necessary), the $\bar{\bar{\mathbf{R}}}$ matrix for open Γ contains rows of zeros with indices corresponding to columns of $\bar{\bar{\mathbf{Z}}}^b$ pointing to barycentric half-RWGs. The mixed Gram matrix $\bar{\bar{\mathbf{G}}}$, required in the definition of $\bar{\bar{\mathbf{Q}}}$, now has additional rows and columns due to the presence of half-RWGs. It can easily be obtained, like in the closed structure case, from analytic expressions.

V. NONUNIFORM DISCRETIZATION DENSITIES

In most practical cases, it is necessary to deal with discretizations that are not only dense, but also nonuniform. This often happens when analyzing electrically large objects with localized fine geometric features. In this case, the discretization of this region can be orders of magnitude denser than that on the rest of the structure. Under these circumstances, minor modifications are required to the method presented in Sections III and IV.

The spectrum of the matrix

$$\left(\bar{\bar{\mathbf{G}}}_m^T\right)^{-1}\bar{\bar{\mathbf{Z}}}_{\mathrm{BC}}\bar{\bar{\mathbf{G}}}_m^{-1}\bar{\bar{\mathbf{Z}}} \tag{58}$$

where

$$\left(\bar{\bar{\mathbf{G}}}_m^T\right)_{i,j}=\left(\bar{\bar{\mathbf{G}}}_m\right)_{j,i}=\langle\hat{\boldsymbol{n}}_{\boldsymbol{r}}\times\boldsymbol{f}_j,\boldsymbol{f}_{\mathrm{BC}i}\rangle=-\langle\hat{\boldsymbol{n}}_{\boldsymbol{r}}\times\boldsymbol{f}_{\mathrm{BC}i},\boldsymbol{f}_j\rangle \tag{59}$$

converges to the spectrum of the operator $\mathcal{T}^2$ in (11) (as the leftmost Gram matrix restores the orthonormality between the source and test functions) and thus the matrix is well conditioned for both uniform and nonuniform discretizations. We may obtain the desired modification to the CMP for nonuniform discretizations using (58) instead of (15). Fortunately, the inversion of $\bar{\bar{\mathbf{G}}}_m^T$ is not really necessary. In fact, consider a nonsingular matrix $\bar{\bar{\mathbf{Y}}}\in\mathbb{R}^{N\times N}$; a simple property of condition numbers ensures that [13]

$$\begin{aligned}&k\left(\bar{\bar{\mathbf{Y}}}\bar{\bar{\mathbf{Z}}}_{\mathrm{BC}}\bar{\bar{\mathbf{G}}}_m^{-1}\bar{\bar{\mathbf{Z}}}\right)\\&\quad=k\left(\bar{\bar{\mathbf{Y}}}\bar{\bar{\mathbf{G}}}_m^T\left(\bar{\bar{\mathbf{G}}}_m^T\right)^{-1}\bar{\bar{\mathbf{Z}}}_{\mathrm{BC}}\bar{\bar{\mathbf{G}}}_m^{-1}\bar{\bar{\mathbf{Z}}}\right)\\&\quad<k\left(\bar{\bar{\mathbf{Y}}}\bar{\bar{\mathbf{G}}}_m^T\right)k\left(\left(\bar{\bar{\mathbf{G}}}_m^T\right)^{-1}\bar{\bar{\mathbf{Z}}}_{\mathrm{BC}}\bar{\bar{\mathbf{G}}}_m^{-1}\bar{\bar{\mathbf{Z}}}\right).\end{aligned} \tag{60}$$

This implies that the matrix $\bar{\bar{\mathbf{Y}}}\bar{\bar{\mathbf{Z}}}_{\mathrm{BC}}\bar{\bar{\mathbf{G}}}_m^{-1}\bar{\bar{\mathbf{Z}}}$ is well conditioned provided that the matrix $\bar{\bar{\mathbf{Y}}}\bar{\bar{\mathbf{G}}}_m^T$ is well conditioned. In the case of a uniform discretization, the matrix $\bar{\bar{\mathbf{G}}}_m$ (and thus $\bar{\bar{\mathbf{G}}}_m^T$) is provably well conditioned [10] and thus $\bar{\bar{\mathbf{Y}}}$ can be set equal to the identity. This justifies the use of (15) in the case of uniform discretizations. In the case of nonuniform discretizations, however, the (nearly diagonal) matrix $\bar{\bar{\mathbf{G}}}_m$ has an ill-scaled diagonal and thus tends to be increasingly ill-conditioned as the ratio between the maximum and minimum mesh edge length increases. This problem can be simply solved by diagonally preconditioning $\bar{\bar{\mathbf{G}}}_m$, i.e., by setting

$$(\bar{\bar{\mathbf{Y}}})_{i,j}=(\bar{\bar{\mathbf{D}}})_{i,j}=\begin{cases}\dfrac{1}{(\bar{\bar{\mathbf{G}}}_m)_{i,j}}, & i=j\\ 0, & \text{otherwise.}\end{cases} \tag{61}$$

In other words, $\bar{\bar{\mathbf{D}}}\bar{\bar{\mathbf{G}}}_m$ (and so $\bar{\bar{\mathbf{D}}}\bar{\bar{\mathbf{G}}}_m^T$) is well conditioned and thus (60) implies that

$$\bar{\bar{\mathbf{D}}}\bar{\bar{\mathbf{Z}}}_{\mathrm{BC}}\bar{\bar{\mathbf{G}}}_m^{-1}\bar{\bar{\mathbf{Z}}} \tag{62}$$

is a well-conditioned matrix. Following the steps that turn (15) into (22), it follows that the CMP (22) should be modified to

$$\bar{\bar{\mathbf{D}}}(\bar{\bar{\mathbf{P}}}^T\bar{\bar{\mathbf{Z}}}^b\bar{\bar{\mathbf{Q}}}\bar{\bar{\mathbf{Z}}}^b\bar{\bar{\mathbf{R}}})\bar{\mathbf{I}}=\bar{\bar{\mathbf{D}}}(\bar{\bar{\mathbf{P}}}^T\bar{\bar{\mathbf{Z}}}^b\bar{\bar{\mathbf{Q}}})\bar{\mathbf{V}}^b \tag{63}$$

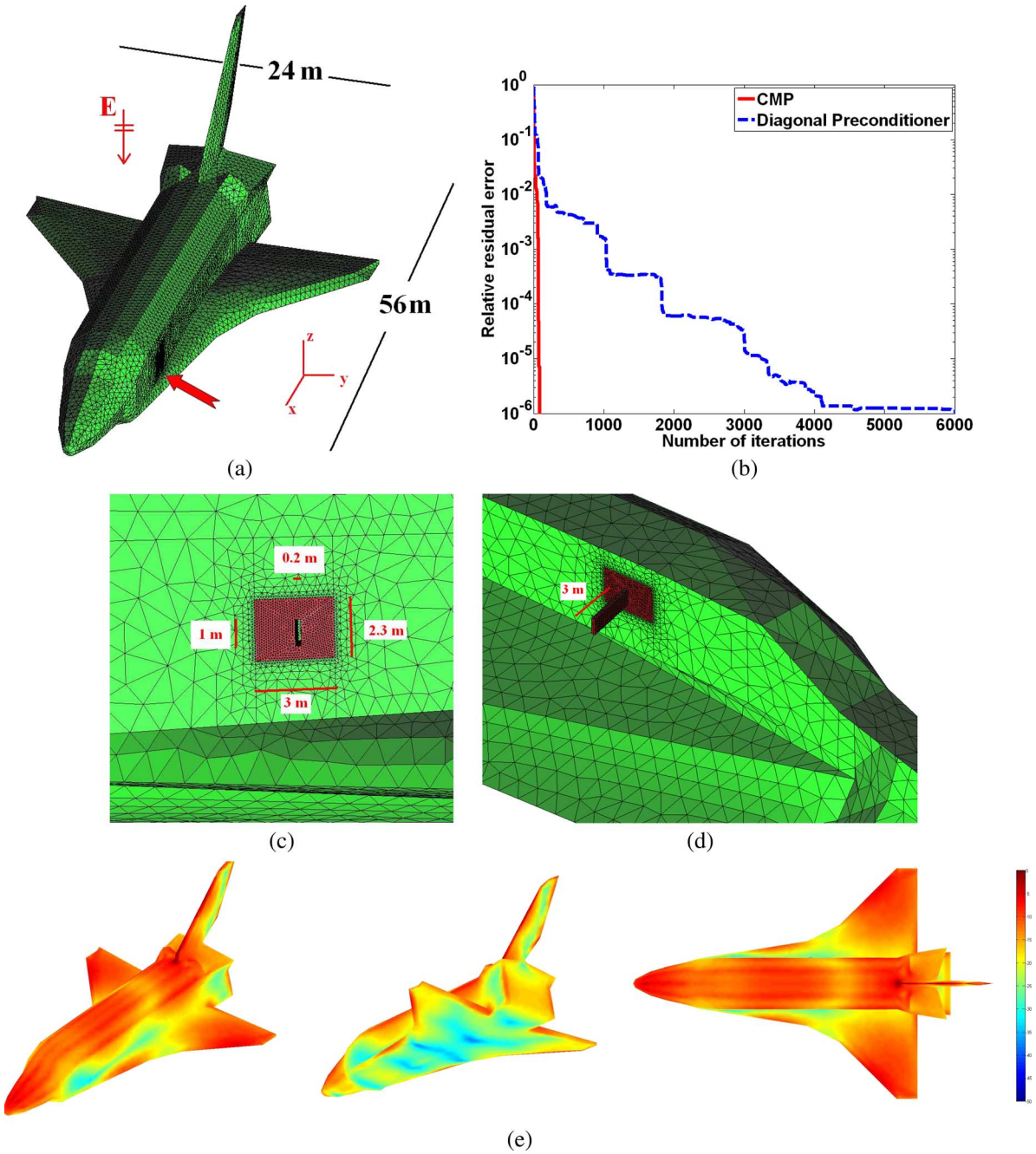

Fig. 10. Analysis of scattering from a space shuttle with a slot waveguide. (a) Problem description. (b) Number of iterations. (c) Slot waveguide detail (outer view). (d) Slot waveguide detail (inner view). (e) Absolute value of the current density induced on the shuttle's surface from three different views (in decibel scale).

to be well conditioned for both uniform and nonuniform discretizations [in fact, (63) becomes equivalent to (22) when the discretization is uniform since $\bar{\bar{\mathbf{D}}}$ is approximately equal to the identity matrix multiplied by a scalar].

The matrix $\bar{\bar{\mathbf{D}}}$ is simply the inverse of the matrix $(\bar{\bar{\mathbf{R}}}^T\bar{\bar{\mathbf{G}}}\bar{\bar{\mathbf{P}}})$'s diagonal in (47) and can be computed in $O(N)$ operations because the matrices $\bar{\bar{\mathbf{R}}}^T$, $\bar{\bar{\mathbf{G}}}$, and $\bar{\bar{\mathbf{P}}}$ have a constant number of elements on every row and on every column. The definition and the computation of the other matrices required by (63) remains unchanged from the ones presented in Sections III and IV. The sole exception is the solution of the linear system in (50), which is necessary in the computation of $\bar{\bar{\mathbf{Q}}}$; the auxiliary linear system

$$\bar{\bar{\mathbf{D}}}(\bar{\bar{\mathbf{R}}}^T\bar{\bar{\mathbf{G}}}\bar{\bar{\mathbf{P}}})\bar{\mathbf{x}} = \bar{\bar{\mathbf{D}}}\bar{\mathbf{y}} \tag{64}$$

should be solved instead to ensure a well-conditioned right-hand side matrix $\bar{\bar{\mathbf{D}}}(\bar{\bar{\mathbf{R}}}^T\bar{\bar{\mathbf{G}}}\bar{\bar{\mathbf{P}}}) = \bar{\bar{\mathbf{D}}}\bar{\bar{\mathbf{G}}}_m$.

VI. Numerical Results

This section presents several examples that demonstrate the effectiveness of the proposed preconditioning scheme and its applicability to complex problems. The results presented here are obtained using a parallel and adaptive integral method (AIM) accelerated EFIE MoM solver [21], which uses the proposed CMP or a standard diagonal preconditioner [22]. This solver uses a transpose-free quasiminimal residual (TFQMR)-based iterative method [23] to solve the EFIE MoM systems. Where not otherwise specified, the CMP formulation in (22) has been used. All simulations were carried out on a

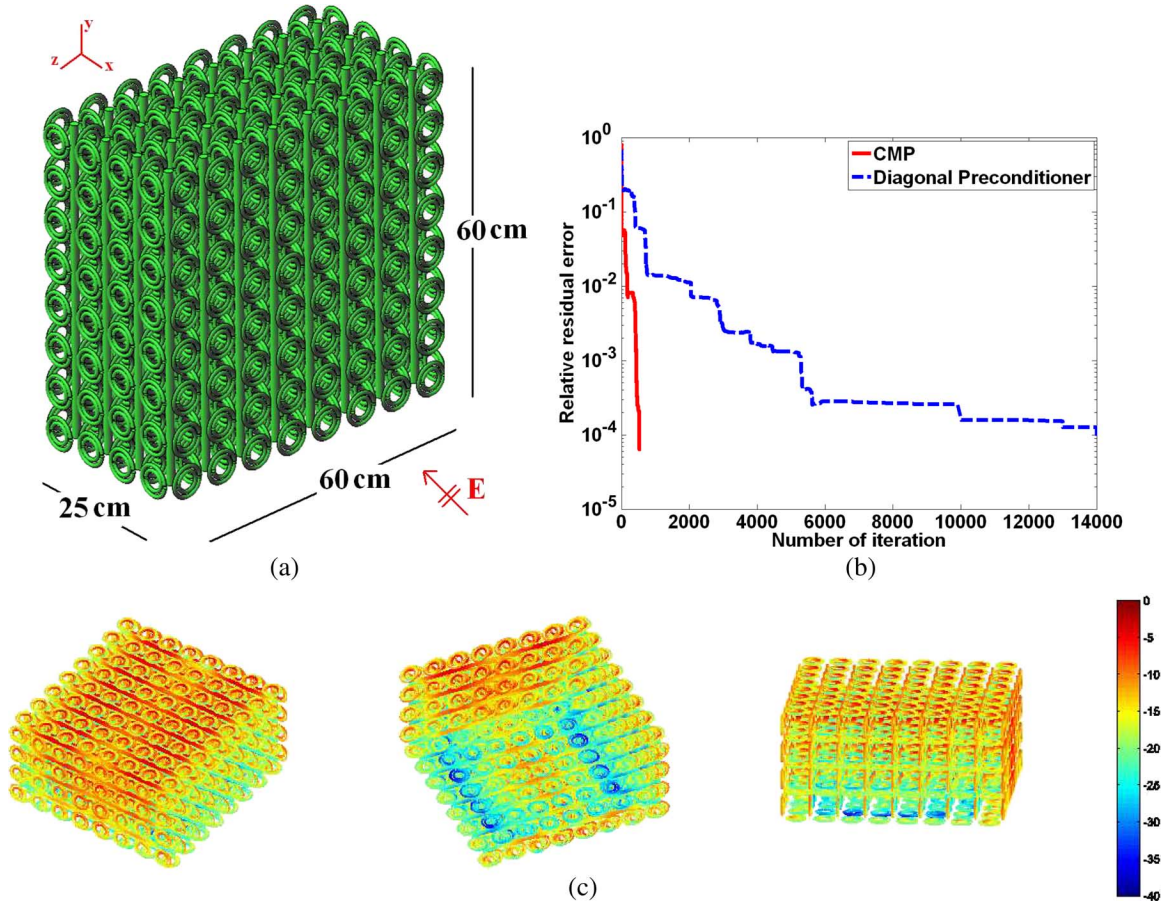

Fig. 11. Analysis of scattering from a split-ring wire metamaterial. (a) Problem description. (b) Number of iterations. (c) Absolute value of the current density induced on the surfaces of rings and wires from three different views (in decibel scale).

cluster of dual-core 2.8-GHz AMD Opteron 2220 SE processors located at the Center for Advanced Computing, University of Michigan (Ann Arbor, MI).

A. *Sphere*

This section demonstrates the benefits of the proposed scheme when applied to closed structures. A sphere of radius $R = \lambda/20$ is excited by a z polarized planewave incident from the $-x$ direction. The simulation is repeated for seven uniform discretizations with element size changing from $\delta = 0.00115\lambda$ to $\delta = 0.02\lambda$. The numbers of standard RWG functions for the densest and coarsest (nonbarycentric) meshes are $N = 502\,000$ and $N = 89$, respectively. Fig. 8(a) presents the condition numbers of the diagonal-preconditioned and CMP-preconditioned EFIE MoM matrices versus δ. Note that because the computation of the condition number of large matrices is very costly, only those of matrices for the five coarsest meshes are presented. As is clearly seen in the figure, even for moderately dense discretizations, the condition number of the diagonal-preconditioned EFIE MoM matrix is orders of magnitude larger than that of the CMP-preconditioned EFIE one. Fig. 8(b) shows the number of iterations required for the relative residual error of the MoM systems' solutions to reach 10^{-6}. In agreement with the condition numbers presented in Fig. 8(a), the number of iterations required to solve the diagonal-preconditioned EFIE MoM system is reduced by approximately 15 times at $\delta = 0.02\lambda$ and approximately 120 times at $\delta = 0.00375\lambda$ (second densest mesh). Note that for the densest mesh, the iterative solver did not converge in 5000 iterations while solving the diagonal-preconditioned EFIE MoM system; on the other hand, the solution of CMP-preconditioned EFIE MoM system still required only ten iterations. Fig. 8(b) shows that the CMP compares favorably also with an incomplete LU preconditioning. Note that the iterative solution of the incomplete LU system matrices requires an increasing number of iterations for increasing mesh density. The high cost of the incomplete LU preconditioning allows only the comparison for the five coarsest meshes. To demonstrate the accuracy of proposed preconditioning scheme, the radar cross sections obtained by solving the diagonal- and CMP-preconditioned EFIE MoM systems at $\delta = 0.00375\lambda$ are compared in Fig. 8(c). The relative norm of the difference between the two curves is less than 0.1%. Table I compares the CPU times required for the solution of the diagonal- and CMP-preconditioned EFIE MoM systems for different discretization densities demonstrating the benefits of the proposed preconditioning scheme.

B. *Plate*

This section demonstrates the effectiveness of the proposed scheme when applied to open structures. A plate with side length $L = \lambda/10$ resides in the xy-plane and its sides are aligned with the $x - y$ coordinate axes. The plate is excited by an y-polarized planewave incident from the z-direction. The simulation is repeated for six uniform discretizations with element size changing

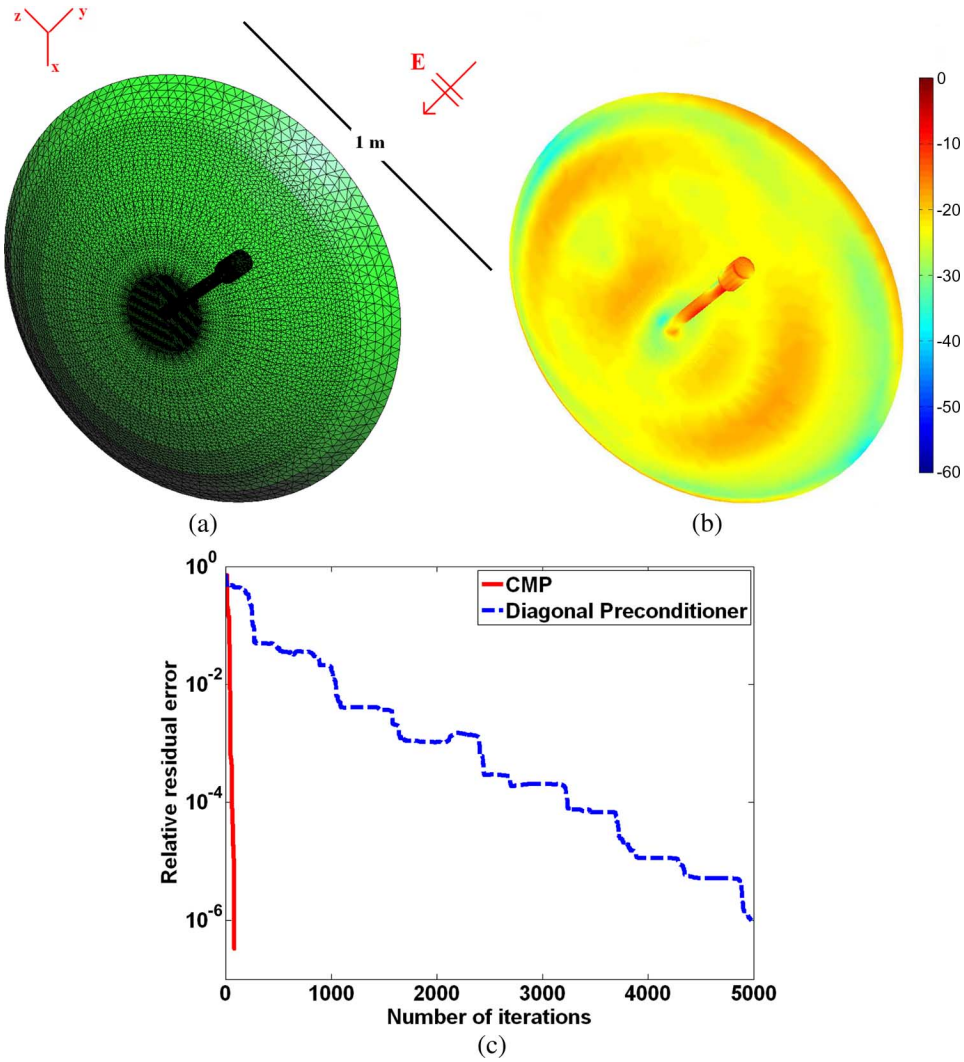

Fig. 12. Analysis of scattering from radar dish. (a) Problem description. (b) Absolute value of the current density induced on the radar dish's surface from three different views (in decibel scale). (c) Number of iterations.

from $\delta = 0.00018\lambda$ to $\delta = 0.0018\lambda$. The numbers of standard RWG functions for the densest and coarsest (nonbarycentric) meshes are $N = 550\,930$ and $N = 13\,250$, respectively. Fig. 9 shows the number of iterations required for the relative residual error of the MoM systems' solutions to reach 10^{-6}. The relative norm of the difference between the solutions of the diagonal- and CMP-preconditioned EFIE MoM systems is less than 0.5%. Table II compares the CPU times required for the solution of the diagonal- and CMP-preconditioned EFIE MoM systems for different discretization densities demonstrating the benefits of the proposed preconditioning scheme.

C. Space Shuttle

This section demonstrates the applicability of the proposed scheme to realistic structures through the analysis of scattering from a space shuttle model [Fig. 10(a)] excited by an x-polarized planewave incident from z-direction at frequency $f = 15$ MHz. The shuttle length is 3λ at the frequency of excitation. A slot and waveguide are located on one side of the shuttle's fuselage, evidenced by an arrow in Fig. 10(a) and detailed in Fig. 10(c) and (d). The shuttle is discretized with an average element size around $\lambda/10$, except for the region near the slot and waveguide, where the average element size is around $\lambda/1200$. The number of standard RWG functions is $N = 29\,409$. Because the discretization is nonuniform, the CMP (63) has been used. The iterative solver required 6032 and 89 iterations for the relative residual error of the diagonal- and CMP-preconditioned EFIE MoM systems' solutions to reach 10^{-6} [Fig. 10(b)]. The CPU times required for the solution of the diagonal- and CMP-preconditioned EFIE MoM systems are 10 h 18 m and 53 m, respectively. Fig. 10(e) shows the absolute value of the current induced on the shuttle's surface in decibel scale from three different views. The relative norm of the difference between the solutions of the diagonal- and CMP-preconditioned EFIE MoM systems is 0.1024%.

D. Split-Ring/Wire Metamaterial

This section demonstrates the applicability of the proposed scheme to realistic structures through the analysis of scattering from a block of split-ring/wire metamaterial [Fig. 11(a)]. The metamaterial is excited by an z-polarized planewave incident from the x-direction at frequency $f = 942$ MHz. The dimensions of the metamaterial blocks are $1.9\lambda \times 1.9\lambda \times 0.7\lambda$. The minimum element size of the discretization is around $\lambda/90$ at the frequency

of excitation. The number of standard RWG functions for this discretization is $N = 614\,088$. The iterative solver required 14 250 and 447 iterations for the relative residual error of the diagonal- and CMP-preconditioned EFIE MoM systems' solutions to reach 10^{-4} [Fig. 11(b)]. The CPU times required for the solution of the diagonal- and CMP-preconditioned EFIE MoM systems are 12 h 40 m and 2 h 7 m, respectively. Fig. 11(c) shows the absolute value of the current induced on the surfaces of rings and wires in decibel scale from three different views. The relative norm of the difference between the solutions of the diagonal- and CMP-preconditioned EFIE MoM systems is 0.3587%.

E. Radar Dish

This section demonstrates the applicability of the proposed scheme to open and realistic structures. A radar dish [Fig. 12(a)] is excited by an z-polarized planewave incident from the y-direction at frequency $f = 1.2$ GHz; the dish diameter is 4λ at the frequency of excitation. The maximum and minimum edge sizes of the discretization are around $\lambda/10$ and $\lambda/650$, respectively. The number of standard RWG functions is $N = 47\,009$. The need for fine discretization is justified by the need of properly modeling the curvature of the radar central feed. Because the radar dish is nonuniformly discretized, the CMP (63) has been used. The iterative solver required 3251 and 60 iterations for the relative residual error of the diagonal- and CMP-preconditioned EFIE MoM systems' solutions to reach 10^{-6} [Fig. 12(c)]. The CPU times required for the solution of the diagonal- and CMP-preconditioned EFIE MoM systems are 4 h 55 m and 38 m, respectively. Fig. 12(b) shows the absolute value of the current induced on the radar dish's surface in decibel scale. The relative norm of the difference between the solutions of the diagonal- and CMP-preconditioned EFIE MoM systems is 0.1639%.

VII. Conclusion

A multiplicative preconditioner for the EFIE has been presented. Leveraging the Calderón identities, the preconditioner ensures fast convergence rates of the MoM iterative solutions even in the presence of dense meshes. Numerical results confirm the effectiveness of the proposed preconditioner and its applicability to complex and realistic structures. Extensions of the proposed approach to deal with junctions and high-order basis functions are feasible and being developed. In addition, the ideas presented here are being modified to construct resonance-free integral equations for PEC and dielectric scattering.

Acknowledgment

The authors would like to thank anonymous reviewers for improving this work with their helpful comments and suggestions.

References

[1] R. F. Harrington, *Field Computation by Moment Method*. Piscataway, NJ: IEEE press, 1993.

[2] R. Coifman, V. Rokhlin, and S. Wandzura, "The fast multipole method for the wave equation: A pedestrian prescription," *IEEE Antennas Propag. Mag.*, vol. 35, no. 3, pp. 7–12, Jun. 1993.

[3] C.-C. Lu and W. Chew, "A multilevel algorithm for solving a boundary integral equation of wave scattering," *Microw. Opt. Technol. Lett.*, vol. 7, no. 10, pp. 466–470, 1994.

[4] E. Michielssen and A. Boag, "A multilevel matrix decomposition algorithm for analyzing scattering from large structures," *IEEE Trans. Antennas Propag.*, vol. 44, no. 8, pp. 1086–1093, Aug. 1996.

[5] J.-C. Nedéléc, *Acoustic and Electromagnetic Equations*. New York: Springer-Verlag, 2000.

[6] R. J. Adams, "Physical and analytical properties of a stabilized electric field integral equation," *IEEE Trans. Antennas Propag.*, vol. 52, no. 2, pp. 362–372, Feb. 2004.

[7] H. Contopanagos, B. Dembart, M. Epton, J. Ottusch, V. Rokhlin, J. Visher, and S. M. Wandzura, "Well-conditioned boundary integral equations for three-dimensional electromagnetic scattering," *IEEE Trans. Antennas Propag.*, vol. 50, no. 12, pp. 1824–1930, Dec. 2002.

[8] S. H. Christiansen and J.-C. Nedelec, "A preconditioner for the electric field integral equation based on Calderon formulas," *SIAM J. Numer. Anal.*, vol. 40, no. 3, pp. 1100–1135, 2003.

[9] S. Borel, D. P. Levadoux, and F. Alouges, "A new well-conditioned Integral formulation for Maxwell equations in three dimensions," *IEEE Trans. Antennas Propag.*, vol. 53, no. 9, pp. 2995–3004, Sep. 2005.

[10] A. Buffa and S. Christiansen, "A dual finite element complex on the barycentric refinement," *Math. Comput.*, vol. 76, pp. 1743–1769, 2007.

[11] Q. Chen and D. R. Wilton, "Electromagnetic scattering by three-dimensional arbitrary complex material/conducting bodies," in *Proc. Antennas Propag. Soc. Int. Symp.*, 1990, pp. 590–593.

[12] S. M. Rao, D. R. Wilton, and A. W. Glisson, "Elettromagnetic scattering by surfaces of arbitrary shape," *IEEE Trans. Antennas Propag.*, vol. AP-30, no. 3, pp. 409–418, May 1982.

[13] G. H. Golub and C. F. van Loan, *Matrix Computation*. Baltimore, MD: The Johns Hopkins University Hospital, 1989.

[14] O. Axelsson, *Iterative Solution Methods*. Cambridge, U.K.: Cambridge Univ.Press, 1994.

[15] J. R. Rice, "A theory of condition," *SIAM Numer. Anal.*, vol. 3, no. 2, pp. 287–310, 1966.

[16] G. C. Hsiao and R. E. Kleinman, "Mathematical foundation for error estimation in numerical solution of integral equations in electromagnetics," *IEEE Trans. Antennas Propag.*, vol. 45, no. 3, pp. 316–328, Mar. 1997.

[17] A. A. Ergin, B. Shanker, and E. Michielssen, "Fast evaluation of three-dimensional transient wave fields using diagonal translation operators," *J. Comput. Phys.*, vol. 146, no. 1, pp. 157–180, 1998.

[18] S. Lang, *Algebra*. New York: Springer-Verlag, 2005.

[19] G. Vecchi, "Loop star decomposition of basis functions in the discretization of the EFIE," *IEEE Trans. Antennas Propag.*, vol. 47, no. 2, pp. 339–346, Feb. 1999.

[20] K. Cools, F. P. Andriulli, F. Olyslager, and E. Michielssen, "Time-domain Calderóon identities and their application to the transient analysis of scattering by 3D PEC objects part II: Stability," *IEEE Trans. Antennas Propag.*, 2007, submitted for publication.

[21] E. Bleszynski, M. Bleszynski, and T. Jaroszewicz, "AIM: Adaptive integral methods for solving large-scale electromagnetic scattering and radiation problems," *Radio Sci.*, vol. 31, no. 5, pp. 1225–1251, 1996.

[22] A. F. Peterson, S. L. Ray, and R. Mittra, *Computational Methods for Electromagnetics*. Piscataway, NJ: IEEE Press, 1998.

[23] R. W. Freund, "A transpose-free quasi-minimal residual algorithm for non-Hermitian linear systems," *SIAM J. Sci. Stat. Comput.*, vol. 14, no. 2, pp. 470–482, 1993.

Francesco P. Andriulli received the Laurea degree in electrical engineering from the Politecnico di Torino, Torino, Italy, in 2004, the M.S. degree in electrical engineering and computer science from the University of Illinois, Chicago, in 2004, and the Ph.D. degree in electrical engineering from the University of Michigan, Ann Arbor, in 2008.

Since 2008, he has been a Research Fellow with the Politecnico di Torino. His research interests are in computational electromagnetic with focus on preconditioning and fast solution of frequency and time-domain integral equations, integral equation theory, hierarchical techniques, integral identities, and single source integral equations.

Dr. Andriulli is the first prize recipient of the student paper competition at the 2007 URSI North American Radio Science Meeting and he has been awarded with the University of Michigan International Student Fellowship and with the University of Michigan Horace H. Rackham Predoctoral Fellowship.

Kristof Cools was born in Merksplas, Belgium, in 1981. He received the M.S. degree in physical engineering from Ghent University, Ghent, Belgium, in 2004. His M.S. thesis dealt with the full wave simulation of metamaterials using the low-frequency multilevel fast multipole method. Since 2004, he has been working towards the Ph.D. degree at the Ghent University under the advisership of Prof. F. Olyslager (Ghent University) and Prof. E. Michielssen (University of Michigan).

Since August 2004, he has been with the Electromagnetics Group of the Department of Information Technology (INTEC), Ghent University. His research focuses on the spectral properties of the boundary integral operators of electromagnetics.

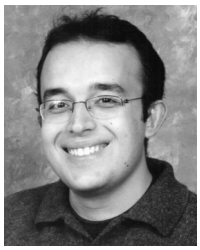

Hakan Bağci received the B.S. degree in electrical and electronics engineering from Bilkent University, Ankara, Turkey, in June 2001 and the M.S. and Ph.D. degrees in electrical and computer engineering from the University of Illinois at Urbana-Champaign (UIUC), Urbana, in August 2003 and January 2007, respectively.

From June 1999 to July 2001, he worked as an Undergraduate Researcher at the Computational Electromagnetics group of Bilkent University. From August 2001 to January 2007, he was a Research Assistant at the Center for Computational Electromagnetics and Electromagnetics Laboratory at UIUC. Since January 2007, he has been a Research Fellow at the Radiation Laboratory, University of Michigan, Ann Arbor. His research interests include various aspects of computational electromagnetics with emphasis on time-domain integral equations and their fast marching-on-in-time-based solutions, developing fast hybrid methods for analyzing EMC/EMI phenomena on complex platforms loaded with cables and circuits, and well-conditioned integral equations.

Dr. Bağci was the recipient of the 2004–2005 Interdisciplinery Graduate Fellowship from the Computational Science and Engineering Department at UIUC. He was also one of the finalists in the student paper competition at IEEE APS symposium in 2005.

Femke Olyslager (S'90–M'93–SM'99–F'05) was born in 1966. She received the M.S. and Ph.D. degrees in electrical engineering from Ghent University, Ghent, Belgium, in 1989 and 1993, respectively.

Currently, she is a Full Professor in Electromagnetics at Ghent University. She authored or coauthored more than 250 papers in journals and proceedings. She coauthored *Electromagnetic and Circuit Modeling of Multiconductor Transmission Lines* (Oxford, U.K.: Oxford Univ. Press, 1993) and authored *Electromagnetic Waveguides and Transmission Lines* (Oxford, U.K.: Oxford Univ. Press, 1999). Her research concerns different aspects of theoretical and numerical electromagnetics.

Dr. Olyslager is Assistant Secretary General of the International Union of Radio Science (URSI), an Associate Editor of the IEEE TRANSACTIONS ON ANTENNAS AND PROPAGATION, and was an Associate Editor of *Radio Science*. In 1994, she became laureate of the Royal Academy of Sciences, Literature and Fine Arts of Belgium. She received the 1995 IEEE Microwave Prize for the best paper published in the 1993 IEEE TRANSACTIONS ON MICROWAVE THEORY AND TECHNIQUES and the 2000 Best Transactions Paper award for the best paper published in the 1999 IEEE TRANSACTIONS ON ELECTROMAGNETIC COMPATIBILITY. In 2002, she received the Issac Koga Gold Medal at the URSI General Assembly, and in 2004, she became laureate of the Royal Flemish Academy of Belgium.

Annalisa Buffa received the Ph.D. degree in mathematics from the University of Milan, Milan, Italy, in 2000 and Dr.Sc. degree in computer science engineering from the University of Pavia, Pavia, Italy, in 1996.

From 2001 to 2004, she was a Researcher in Applied Mathematics at the Institute of Numerical Analysis, Italian National Research Council (CNR), Pavia, Italy. Since 2004, she has been a Research Director (equivalent to full Professor) at the Institute of Applied Mathematics and Information Technology, CNR. Since 2001, she has been an Invited Professor in several Universities such as ETH-Zurich, Switzerland, Ecole Polytechnique and University of Paris VI, France, and ICES-University of Texas at Austin. She has coauthored more than 40 papers in journals with international editorial board on different subjects of applied mathematics, numerical analysis and computational electromagnetism. Currently, her main scientific interests are in the field of computational electromagnetism with variational techniques, i.e., finite and boundary elements. She works actively on the definition and the mathematical well posedness of integral equations for electromagnetic wave propagation in exterior domains, in presence of dielectric interfaces and antennas, and eigenvalues problems for waveguides. In the past, she worked intensively on discretization methods for eddy-currents problems with moving geometries, and on mathematical justifications of low-frequency models in electromagnetics.

Snorre Christiansen was born 1975 in Oslo, Norway. He graduated from Ecole Polytechnique, Paris, France, in 1997 and received the Ph.D. degree in applied mathematics in 2002. His supervisor was J. C. Nédélec.

Since 2006 he has been an Associate Professor at the Center of Mathematics for Applications, University of Oslo.

Dr. Christiansen received a European Young Investigator (EURYI) award in 2005.

Eric Michielssen (M'95–SM'99–F'02) received the M.S. degree in electrical engineering (*summa cum laude*) from the Katholieke Universiteit Leuven (KUL), Leuven, Belgium, in 1987 and the Ph.D. degree in electrical engineering from the University of Illinois at Urbana-Champaign (UIUC), Urbana, in 1992.

He served as a Research and Teaching Assistant in the Microwaves and Lasers Laboratory at KUL and the Electromagnetic Communication Laboratory at UIUC from 1987 to 1988 and from 1988 to 1992, respectively. Following a postdoctoral stint at UIUC, he joined their faculty in the Department of Electrical and Computer Engineering in 1993, reaching the rank of Full Professor in 2002. In 2005, he joined the University of Michigan, Ann Arbor, as Professor of Electrical Engineering and Computer Science. He authored or coauthored over 135 journal papers and book chapters and over 200 papers in conference proceedings. His research interests include all aspects of theoretical and applied computational electromagnetics. His principal research focus has been on the development of fast frequency and time-domain integral-equation-based techniques for analyzing electromagnetic phenomena, and the development of robust optimizers for the synthesis of electromagnetic/optical devices.

Dr. Michielssen served as the Technical Chairman of the 1997 Applied Computational Electromagnetics Society (ACES) Symposium (Review of Progress in Applied Computational Electromagnetics, March 1997, Monterey, CA), and served on the ACES Board of Directors (1998–2001 and 2002–2003) and as ACES Vice-President (1998–2001). From 1997 to 1999, he was as an Associate Editor for Radio Science, and from 1998 to 2005 he served as Associate Editor for the IEEE TRANSACTIONS ON ANTENNAS AND PROPAGATION. He received a Belgian American Educational Foundation Fellowship in 1988 and a Schlumberger Fellowship in 1990. Furthermore, he was the recipient of a 1994 International Union of Radio Scientists (URSI) Young Scientist Fellowship, a 1995 National Science Foundation CAREER Award, and the 1998 Applied Computational Electromagnetics Society (ACES) Valued Service Award. In addition, he was named 1999 URSI United States National Committee Henry G. Booker Fellow and selected as the recipient of the 1999 URSI Koga Gold Medal. He also was awarded the UIUC's 2001 Xerox Award for Faculty Research, appointed 2002 Beckman Fellow in the UIUC Center for Advanced Studies, named 2003 Scholar in the Tel Aviv University Sackler Center for Advanced Studies, and selected as UIUC 2003 University and Sony Scholar. He is a member of URSI Commission B.